

Final version published in Journal of Morphology, 227 (2016). 1168-1186. DOI 10.1002/jmor.20567

# The Nematode Stoma: Homology of Cell Architecture with Improved Understanding by Confocal Microscopy of Labeled Cell Boundaries

A. H. Jay Burr<sup>1,2\*</sup> and James G. Baldwin<sup>2</sup>

<sup>1</sup>Department of Biological Sciences, Simon Fraser University, Burnaby, British Columbia, V5A 1S6, Canada

<sup>2</sup>Department of Nematology, University of California, Riverside, California, 92521

\*Corresponding author: [burr@sfu.ca](mailto:burr@sfu.ca)

**ABSTRACT** Nematode stomas vary widely in the cuticular structures evolved for different feeding strategies, yet the arrangement of the epithelial cell classes that form these structures may be conserved. This article addresses several issues that have impeded the full acceptance of this hypothesis including controversies arising from the structure of the *Caenorhabditis elegans* stoma. We investigated fluorescent antibody labeling of cell boundaries in conjunction with confocal microscopy as an alternative to transmission electron microscopy (TEM), using MH27 to label apical junctions in *C. elegans* and two other species. Accurately spaced optical sections collected by the confocal microscope provide a three-dimensional array of pixels (voxels) that, using image-processing software, can be rotated and sectioned at accurately chosen thicknesses and locations. Ribbons of fluorescence clearly identify cell boundaries along the luminal cuticle in *C. elegans* and *Zeldia punctata* and less clearly in *Bunonema* sp. The patterns render cell classes and their relationships readily identifiable. In the *C. elegans* stoma they correct a misreading of serial TEMs that was not congruent with architecture in other nematodes—the row of marginal cells is now seen to be continuous as in other nematodes, rather than being interrupted by encircling *pm1* cells. Also impeding understanding, the reference to certain cell classes as ‘epithelial’ and others as “muscle” in the *C. elegans* literature is at variance with muscle expression in most other taxa. For consistent comparison among species, we propose that these cell class descriptors based on function be replaced by topological terms. With these and other confusing concepts and terminology removed, the homology of the cellular architecture among taxa becomes obvious. We provide a corrected description of the cell architecture of the *C. elegans* stoma and examples of how it is modified in other taxa with different feeding strategies.

## INTRODUCTION

The cuticular feeding apparatus of the nematode

stoma and pharynx, especially visible in the light microscope because of its strong refraction, is observed in a fascinating variety of forms that reflect diverse feeding strategies among taxa (Kiontke and Fitch, 2013). In addition to a luminal structure and musculature for pumping and suck-ing common to most taxa, adaptations include fixed or moveable teeth for predation or parasit-ism, extendible stylets to aid penetration of hosts or prey and varied expression of muscle for move-ment of valves, grinders, stylets, or teeth.

Over the last two centuries these structures have been important as characters for identifica-tion, classification and hypotheses of phylogenetic relationships (Chitwood and Chitwood, 1950; Maggenti, 1981; De Ley et al., 1995; Sudhaus and Kiontke, 1996; Coomans, 2000; Siddiqi, 2000). In the past two decades a molecular phylogeny has emerged that provides a new framework for interpreting the evolution of these characters (Fig. 1; Blaxter et al., 1998; De Ley and Blaxter, 2002; De Ley, 2006) which has been broadly supported by more recent phylogenetic analyses (see Fig. 1 legend). And in the past four decades the cellular architecture underlying these structures has been reconstructed from transmission electron micrographs (TEMs) in a number of taxa, highlighted by the detailed reconstruction of the entire *Caenorhabditis elegans* stoma and pharynx (Albertson and Thomson, 1976). In a review of the earlier studies, De Ley et al. (1995) proposed that the diversity of musculature and cuticular structure of the stoma is underlain by a conserved cellular

Research supported by a National Science Foundation grant; Grant numbers: DEB 0731516 and DEB 1257331

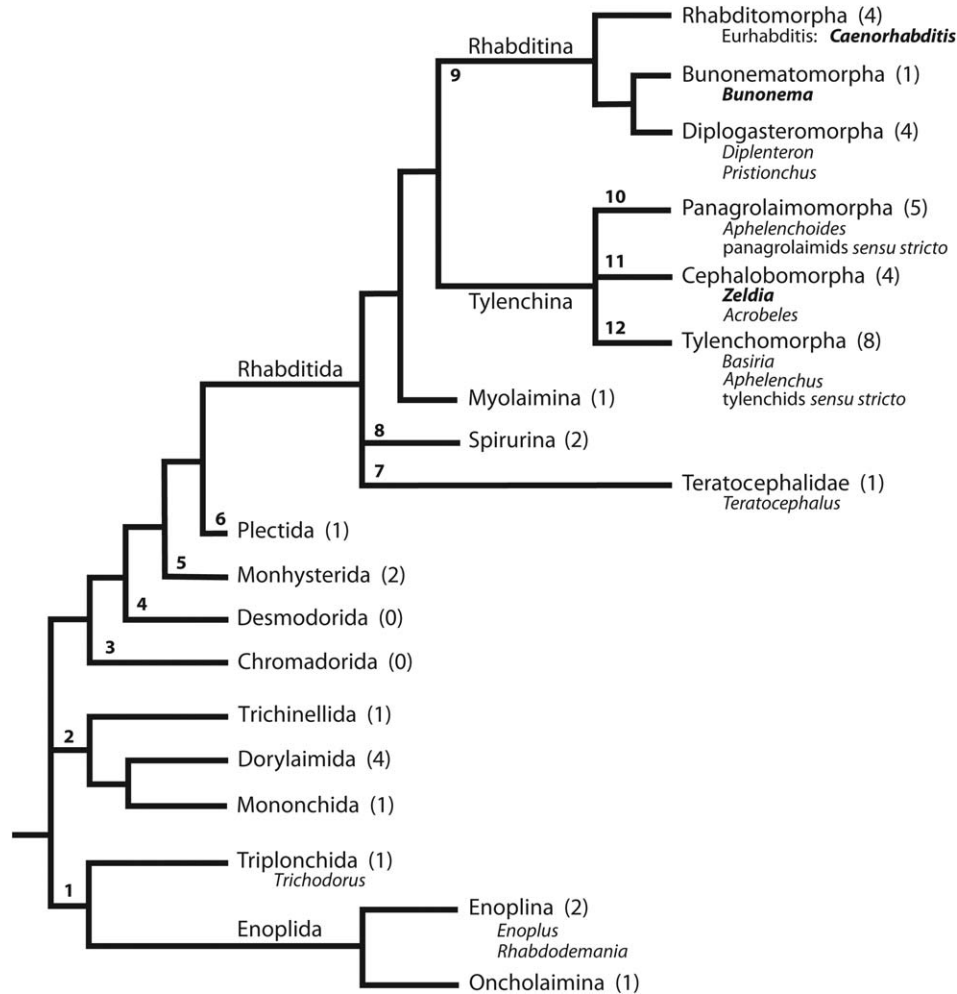


Fig. 1. Nematode phylogeny showing relationships of taxa in which the stoma has been investigated at the TEM level according to our survey of the literature. Parentheses indicate the number of genera investigated in each taxon and the bold font highlights those investigated in this paper. The taxa investigated cover the entire range of nematode taxa but insufficiently for those outside of Rhabditida. Clade numbers are from Holterman et al. (2006). Clade branching and taxon names are primarily according to De Ley (2006) and based on the molecular analysis and classification of De Ley and Blaxter (2002). The branching shown appears to be confirmed by the more extensive molecular analysis of Meldal et al. (2007), van Megen et al. (2009) and Bik et al. (2010). *Aphelenchoides* and *Aphelenchus* are placed in Panagrolaimomorpha and Cephalobomorpha, respectively, consistent with Bert et al. (2008) and van Megen et al. (2009). *Rhabdodemanina* is placed within Enoplida as proposed by Smythe (2015). Eurhabditis, a clade within Rhabditomorpha that includes *C. elegans* and close relatives, is described by Kiontke and Fitch (2005).

architecture: a pattern of distinct cell classes lining the stoma whose sequence along the luminal cuticle is conserved. This hypothesis has been supported by recent studies involving three-dimensional (3D) reconstruction of stomas with otherwise very different morphology and function (Bumbarger et al., 2006; Ragsdale et al., 2008, 2011).

However, full acceptance of the De Ley et al. model has been hindered by the occurrence of exceptional anatomical features in the model nematode, *C. elegans*. One is that pairs of cells in the radial cell row that run between the marginal cell rows in *C. elegans* become interconnected shortly after hatching (Sulston and Horvitz, 1977) and presumably after each molt. Otherwise, these cells retain their morphology and this “fusion” occurs

only in the small clade that includes *C. elegans*. We argue that these “syncytia” should nevertheless be considered as paired cells, and as such the topology conforms to what is observed in other nematodes.

Secondly, acceptance has been hindered by confusion caused by the terms “epithelial” and “muscle” used to distinguish the cell classes in *C. elegans* (Altun and Hall, 2009). These are not universally applicable. In fact, “epithelial” cells *e1* and *e3* are muscular in most nematodes investigated. Both cell classes are non-muscular in only two widely separate taxa: the Rhabditina (which includes *C. elegans* and *Bunonema*), and the Dorylaimida (Fig. 1). On the other hand, the so-called “muscle” cells *pm1* and *pm2* do not express muscle

in the tylenchids *sensu stricto* (Ragsdale et al., 2011). Thus, a terminology based on non-muscular or muscular function is inappropriate and misleading. And classifying *e2* as “epithelial” is confusing because it is identical in form and function to marginal cells *mc1-mc3*. Here, we recommend other terms for distinguishing between cell classes that consistently emphasize a topology that is homologous in all taxa: toroidal, marginal, radial, paired, and unpaired.

A feature of the nematode stoma and pharynx, the continuity of the row of marginal cells, escaped notice in the TEM reconstruction of *C. elegans* by Albertson and Thomson (1976), and the stoma continues to be incorrectly illustrated (e.g., Altun and Hall, 2009). Here, with fluorescent antibody staining and confocal microscopy, we provide new information on the cellular architecture of the stoma in *C. elegans*, including strong evidence that the row of marginal cells includes *e2* and is indeed continuous without interruption by the *pm1* cell processes. In a forthcoming article we will support this observation with a reconstruction from TEMs. Here, we provide a corrected description of the cellular architecture in *C. elegans* and compare it with two other species.

There is a need to test the De Ley et al. (1995) hypothesis in additional taxa. While TEM-reconstructions have expanded our knowledge of character homology and diversity to the cellular level, these new characters have not been explored adequately outside the Rhabditina and Tylenchina clades (Fig. 1). Full comparison across more than a few representative taxa by this approach is limited by its labor-intensive and costly nature. This can result in under-sampling, which can tempt attributing to a clade features that instead are more restricted in distribution. Here we explore the suitability of another approach: fluorescent labeling of cell boundaries and confocal microscopy. These methods have been applied widely in *C. elegans* to follow the development of cellular architecture during embryogenesis (e.g., Portereiko and Mango, 2001), and the postembryonic development of the hypodermis (Podbilewicz and White, 1994), tail region (Fitch and Emmons, 1995; Fitch, 1997), and the vulval region (Sharma-Kishore et al., 1999; Kolotuev and Podbilewicz, 2008). However, these procedures have not been applied previously to investigations of the stoma and anterior pharynx in *C. elegans* and not at all in other nematodes.

We investigated the applicability of fluorescent labeling and confocal microscopy to two species for which the stoma has been previously reconstructed by TEM, using *C. elegans* as a reference species. In this way we assessed the competence of the confocal data in the stoma and anterior pharynx and whether these structures are phylogenetically informative. We adapted the protocol developed by Finney and Ruvkun (1990) and

modified by Fitch and Emmons (1995) for staining apical junctions (AJs) in *C. elegans* (syn.: adherens junctions, CeAJs) with fluorescent-labeled MH27. This is an antibody to the AJM-1 protein in AJs that border epithelial cells (Francis and Waterston, 1991; Köppen et al., 2001; Labouesse, 2006). We compared confocal microscopy with epifluorescence microscopy, finding advantages to the former. In addition to its higher resolution and contrast, the confocal microscope provides a precise 3D voxel array of the architecture that can be manipulated with image processing software to isolate regions and sections of interest. This enabled accurate mapping of the cellular architecture around the stoma lumen. To our knowledge the latter feature of confocal microscopy has not previously been applied in studies of cellular architecture in any organism.

Beginning with the work of De Ley et al. (1995), a new concept is emerging: that the highly diverse cuticular structures and different feeding strategies, long observed across Nematoda, appear to have evolved by modifying the expression of a conserved template of ordered cell classes. The pharyngeal template is formed during embryogenesis as shown in *C. elegans* (Sulston et al., 1983; Rasmussen et al., 2008, 2012, 2013). Such a mechanism of morphological evolution appears to be highly adaptable yet conservative across deep phylogenetic divergences. Details can be sought in a few representative taxa by 3D TEM reconstructions, as done for *Aphelenchus avenae* (Ragsdale et al., 2011) and *Acrobeles complexus* (Bumbarger et al., 2006). But there needs to be a broader survey of taxa that takes advantage of the more time- and cost-efficient approach we report here: fluorescent labeling of cell boundaries and confocal microscopy. Further sampling could strengthen the hypothesis that the template of ordered cell classes is ancestral within nematodes and may reveal interesting variations on this pattern.

## MATERIAL AND METHODS

### Source and Cultivation of Specimens

*Caenorhabditis elegans* N2 strain, provided by Morris Maduro, was cultivated on NGM agar plates coated with *Escherichia coli* mutant OP50 (Brenner, 1974). In the Baldwin lab *Bunonema* sp. (JB116), an undescribed species, was similarly cultured (Dolinski and Baldwin, 2003), whereas *Zeldia punctata* (JB015) was maintained on water agar seeded with *E. coli* OP50 (Zhang and Baldwin, 2000). The *C. elegans* GFP-apical junction marker strain JR1000 that contains *ajm-1::GFP* was made by Morris Maduro and obtained from the *C. elegans* Genetics Center (funded by NIH Office of Research Infrastructure Programs, P40 OD010440).

### Preparing Specimens for Confocal Microscopy

The protocol used was developed for *C. elegans* by Finney and Ruvkun (1990), modified by Fitch and Emmons (1995) and here adapted for work with other nematode species. For details

see supplementary online material text-S1. The procedure carries the worms in Eppendorf centrifuge tubes through fixation, freeze–thaw, permeabilization, and antibody-binding steps. The fixative was 1% paraformaldehyde and 20% methanol in a buffer containing EGTA, PIPES, and spermidine. Permeabilization of the cuticle involved incubation with reducing agents [100 mM (mmol L<sup>-1</sup>) beta-mercaptoethanol in Tris-Triton buffer (100 mM, pH 7.4) then 25 mM dithiothreitol in borate buffer (25 mM, pH 9.2)], then an oxidant (1% H<sub>2</sub>O<sub>2</sub> in borate buffer). They were then passed successively through borate buffer, Antibody Buffer B (10× Ab Stock + 1% BSA), then Antibody Buffer A (1× Ab Stock + 1% BSA) in which they could be stored. Ab Stock consisted of 0.5% Triton X-100, 1 mM EDTA, and 0.5% Na azide in PBS-buffer.

The primary antibody MH27, originating from the Waterston lab (Francis and Waterston, 1991) and donated by David Fitch, was an IgG from a mouse hybridoma cell line. The secondary antibody was an AffiniPure Goat Anti-mouse IgG (H + L)–Cy3 conjugate (Jackson ImmunoResearch Laboratories Inc.). Goat serum was purchased from Roche Applied Science Inc. The worms were incubated for 4 hours or overnight at 37°C in 2% MH27 + 1% goat serum in Antibody Buffer A. After washing 4× at room temperature with Antibody Buffer B, they were incubated at 37°C for 4 hours or overnight in 1% secondary antibody + 1% goat serum in Antibody Buffer A. The worms were then washed 4× with Antibody Buffer B at room T, stored in an equal volume of glycerol-SlowFade (Molecular Probes Inc) and mounted on slides in that medium.

This modified Finney–Ruvkin procedure worked very well with *C. elegans*, producing brightly fluorescent AJs that resisted fading. The morphology of the preparations was not noticeably different from that in specimens of the *C. elegans* strain JR1000, an AJM-1::GFP recombinant, prepared by paraformaldehyde fixation and mounted in glycerol-SlowFade. The fluorescence was weaker and faded more quickly than the antibody-labeled preparation.

*Bunonema* sp. and *Zeldia punctata* appeared not to be permeabilized by the Finney–Ruvkin method—only worms broken during the procedure were labeled. The permeabilization steps could be bypassed by cutting the worms, multiple freeze–thaw cycles in paraformaldehyde/methanol or by splitting worms frozen between microscope slides (Hedgecock et al., 1990). A problem with the latter procedure was distortion of the morphology by flattening of the specimen. This did not interfere with identifying the cell classes or their sequence, but under such conditions rotation of the recorded voxel array would not be fruitful. We did not try laser microbeam puncturing the cuticle for permeabilizing the worms (Cole and Schierenberg, 1986). The results are based on seven well-stained specimens of *Zeldia*, three of *Bunonema* and numerous *C. elegans* hermaphrodites and juveniles.

During many of the procedures, a major problem was losing worms. In order to ensure retention of small numbers of specimens, we tried microcapsules covered with a permeable membrane, both the one developed by Bumbarger et al. (2006) and a similar one made inexpensively from the cap of an 0.5 µl Eppendorf centrifuge tube.

## Electron Microscopy

Transverse TEMs of *C. elegans* (Figs. 3A and 4A,B) were selected from three different sets of serial sections archived in the Worm Image Database ([www.wormimage.org](http://www.wormimage.org)). That of Figure 3A is print 179 (#N2T\_114572) of the “N2T” series originally prepared for Albertson and Thomson (1976) and others in the Brenner lab. Those of Figure 4A,B were modified from prints 3731-19 and 3732-23 (Perkins nose 1\_123675 and 1\_123693), which are transverse sections from of the “Perkins TS” series prepared for, Perkins et al. (1986). The longitudinal TEMs of Figure 3B,D were modified from prints LS\_29a and LS\_29b (merged to print LN-319671) of the “Perkins LS” series prepared for Wright and Thomson (1981). The Perkins LS set

was scanned in the Baldwin lab and archived in the Worm Image Database under the name Lengthwise\_Nose. Each of the three sets had been prepared from a single adult hermaphrodite specimen after fixation with 2% OsO<sub>4</sub>. Procedural details are available from the respective publications. The WormImage Database is maintained for the scientific community by David Hall and supported by NSF grant #NIH OD 010943. David Hall kindly provided us images of higher resolution than downloadable from [wormimage.org](http://wormimage.org).

## Confocal Microscopy

A practical guide for confocal microscopy is provided by Centonze and Pawley (2006). The Leica SP2 UV confocal microscope includes optics for epifluorescence illumination, bright field or DIC. We used a 63×, N.A. 1.2 water immersion lens with different zoom factors for the stoma and entire pharynx. Serial optical sections (spaced by 0.2 µm in *Zeldia* and *C. elegans* and 0.16 µm in *Bunonema*) were obtained at increasing depth, using the motor-controlled stage. Both fluorescent and either DIC or bright-field images were recorded at each focal plane. With the Cy3 fluorophore, green HeNe laser illumination was used with the TRITC filter. With GFP, blue Argon laser illumination was used with the FITC filter. Scanner settings were typically: 1024 × 1024 resolution (200 Hz), 50% beam intensity and line averaging = 2. The pinhole was set at 1.0 for optimum z-resolution. PMT gain was increased until oversaturation just began.

## Image Processing

Most of image processing reported here utilized the open-source application ImageJ, version 1.48a (Wayne Rasband, <http://imagej.nih.gov/ij>), and a set of plugins: ImageJ for Microscopy, collated by Tony Collins and available from The Wright Cell Imaging Facility, Toronto Western Research Institute, [www.uhnresearch.ca/wcif](http://www.uhnresearch.ca/wcif). For descriptions and authorship of plugins see <http://rsbweb.nih.gov/ij/plugins/index.html#stacks>. A more updated version of ImageJ applicable to biological microscopy is Fiji (<http://fiji.sc/Fiji>). For details of tools used in our results see supplementary online material text-S2. For further description of native ImageJ tools see the ImageJ User Guide.pdf and the online (downloadable) manual for ImageJ (<http://imagej.nih.gov/ij/docs/>). Use of MBF plug-ins are described in a short introductory article “ImageJ for Microscopy” (Collins, 2007) and in the Online Manual for the “ImageJ for Microscopy” bundle of plug-ins (<http://fiji.sc/mbf/index.htm>).

**Preparing the image stack for sectioning.** The confocal microscope provided a file folder containing alternating fluorescent and DIC images of optical sections spaced 0.2 µm apart, typically at 100 focal planes. The TIFF images consisted of 512 × 512 pixels and, with the 63× objective, they were spaced 0.074 µm apart (dimensions provided by the confocal microscope application software). Thus the initial voxel dimension was 0.074 × 0.074 × 0.2 µm. Most image processing was done using ImageJ but for Figure 6A–C the recorded image array was cropped, converted to inverted gray-scale and contrast enhanced using LeicaLite, a software application provided with the Leica confocal microscope. Image arrays with equidimensional voxels were prepared before rotating for Figures 5E,F and 8. Arrays for transverse sectioning (Fig. 6D–I) were rotated to a rear-on view before sectioning. Longitudinal and transverse sections of the arrays and cylindrical projections were prepared with ImageJ.

**Volume-rendered 3D-visualization (Fig. 5B).** The freely-available computer application Image Surfer 2 (Feng et al., 2007) was used. The Volume Mapper rendering style was set on Smart. The color scale and opacity scales in Color Map were adjusted by trial and error. See Supporting Information S2 for details. The result has a 3D appearance presumably because the ray-casting algorithm makes voxel values brighter in higher images in the voxel array.

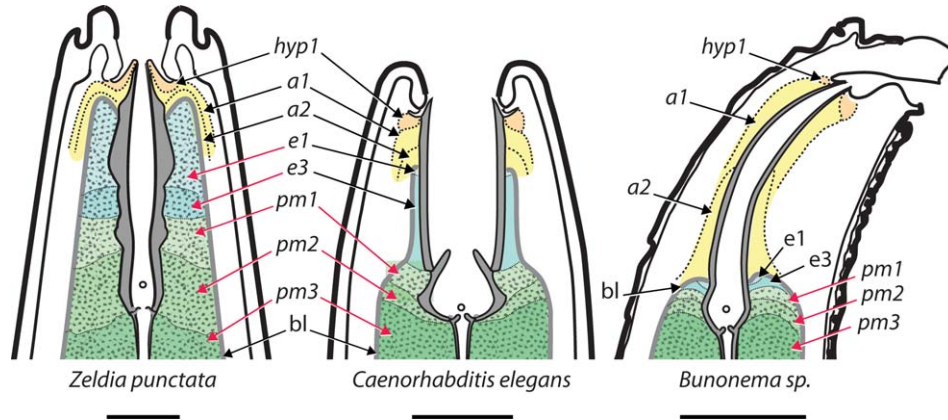


Fig. 2. Comparison of stoma architecture in the three species investigated in this article. The same sequence of epithelial cell classes occur in the three species: toroidal cells *hyp1*, *a1*, *a2* followed by rows of radial cells *e1*, *e3*, *pm1*, and *pm2*. The rows of radial cells in the stoma continue through the pharynx beginning with *pm3*. The cells of the stoma and pharynx are enveloped by a basal lamina beginning with *e1*. Not included in these frontal sections (e.g., Fig. 3A, white line) are the marginal cells *e2* and *mc1* that, posterior to the toroidal cells, separate the cross section into three sectors (see Fig. 3A). Radial cells *e1* and *e3* occur as a single cell in each radial sector and radial cells *pm1*, *pm2* and *pm3* are paired. Whether or not a particular cell class expresses muscle (spotted pattern, red arrows) differs in each species. As hypothesized by De Ley et al. (1995), the same pattern of cell classes occurs in all taxa investigated by TEM (Fig. 1). The drawings are reconstructed from serial transmission electron micrographs (TEMs): *Caenorhabditis elegans* from Figure 3B–D, *Zeldia punctata* from Baldwin and Eddleman (1995) and Dolinski et al. (1998), and *Bunonema* sp. from Dolinski and Baldwin (2003). The position of the dorsal gland orifice in these dorsal views is indicated by the small circle. The architecture of *Bunonema* is here based on a reinterpretation of earlier micrographs in the light of recent observations on other nematode taxa (Baldwin et al., 2004; Ragsdale and Baldwin, 2010; Ragsdale et al., 2008, 2013). Scale bar = 3  $\mu$ m.

**Preparation of illustrations.** TIFF images were cropped, resized and adjusted in brightness and contrast with Photoshop Elements, before “Placing” them into a figure being prepared with Adobe Illustrator. Fine, colored ink marks on the TEM images provided by WormImage were removed from the images under high zoom using the Photoshop Healing Brush tool set at 10 pixel width without noticeably altering details in the micrograph.

## RESULTS

### Cellular Architecture of Nematode Stomas

The objective of this section is to introduce the nematode stoma morphology and nomenclature needed to understand our findings and provide a corrected description of the *C. elegans* stoma. Support for our findings will be presented in the subsequent sections. At the same time, we introduce the modified terminology that we recommend for consistency across Nematoda. The epithelial cell architecture of the three species we investigated is compared in Figure 2 and details of the nematode stoma and procorpus are illustrated further on TEMs of *C. elegans* in Figures 3 and 4. The architecture of pharyngeal gland cells and neurons is not considered in this article as these cells are not outlined by the fluorescent antibody stains—AJs occur only where a gland duct orifice penetrates the luminal cuticle and where a nerve process terminates at the cuticle.

The stoma cuticle anterior to the gymnostom, in the cheilostom region, is continuous with the body cuticle and is secreted by the hypodermal syncytium *hyp1* (Figs. 2 and 3B,C; Wright and

Thomson, 1981; Endo, 1985; Bumbarger et al., 2006). A different cuticle is recognizable posterior to the cheilostom and is formed by the cell classes that make up the pharyngeal tube. The pharyngeal cuticle is continuous from the gymnostom and stegostom of the stoma (Fig. 3B), through the procorpus and other regions of the pharynx (Fig. 5A), then through the pharyngeal-intestinal valve to its junction with the lining of the intestine. The cuticle of the gymnostom is formed by arcade syncytia *a1* and *a2*, which successively envelop the cuticle with a toroidal topology. The cuticle of the stegostom, procorpus and the rest of the pharynx is formed by a single layer of epithelial cells that are enveloped by a common basal lamina and arranged sequentially in rows along the cuticle.

Of interest, the stoma, pharynx and pharyngeal-intestinal valve develop as one unit during embryonic morphogenesis of *C. elegans*. The developing “pharyngeal tube” includes the arcade cells at the anterior end, *pm8* and the cells of the pharyngeal-intestinal valve at the posterior end, and all radial and marginal cell classes between (Portereiko and Mango, 2001; Rasmussen et al., 2008). The pharynx-specifying FoxA transcription factor, Pha-4, is expressed in these cells and not in *hyp1* or the intestinal cells (Mango, 2007, 2009). The cheilostom (formed by *hyp1*), however, is usually included with gymnostom and stegostom in the definition of stoma (De Ley et al., 1995) as it is part of the buccal cavity and may be involved in feeding.

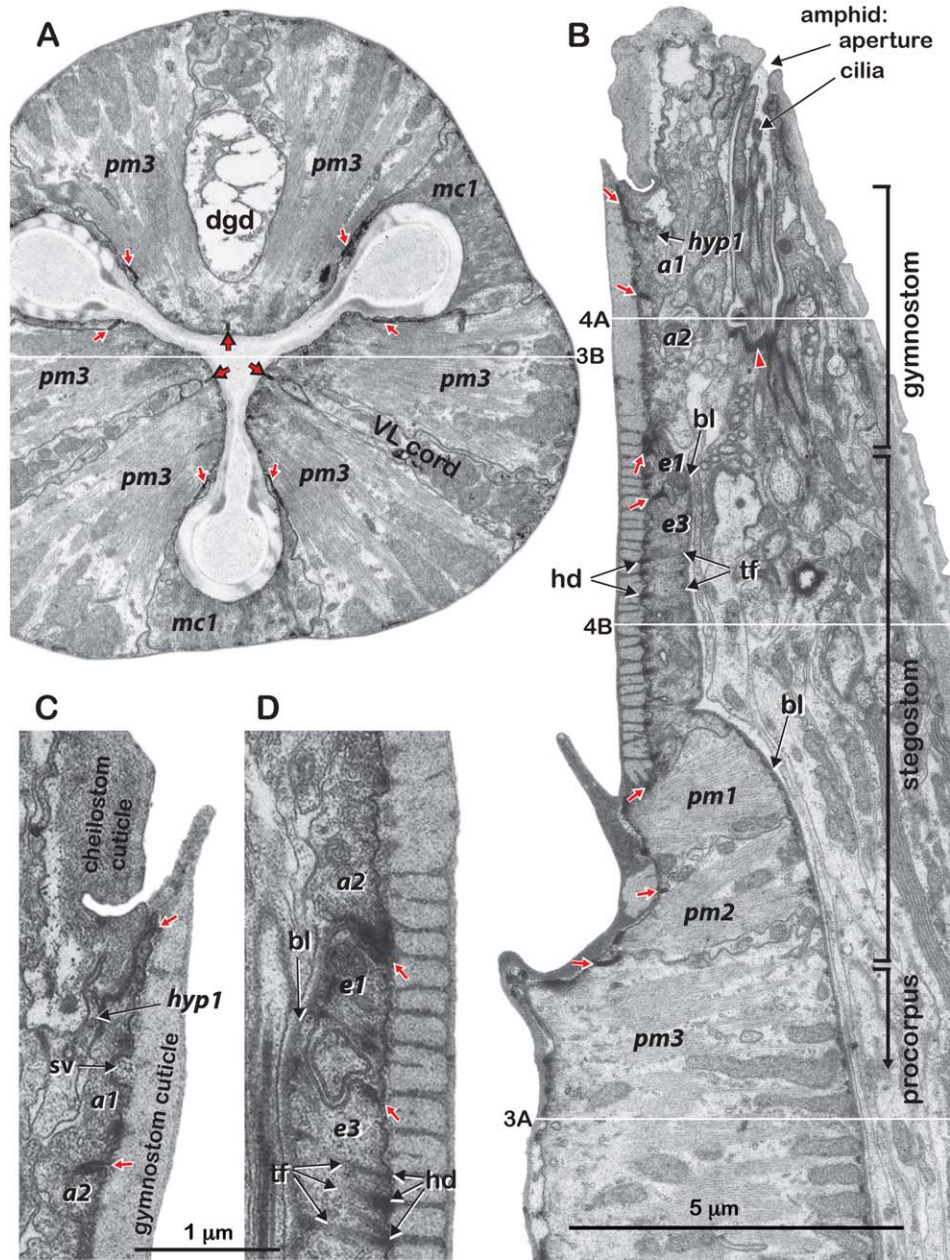


Fig. 3. Stoma architecture in *C. elegans*. Red arrows mark apical junctions, which are cross-sectioned at longitudinal (A) and circumferential (B–D) cell boundaries. These are stained by the fluorescent antibody MH27 in Figures 5–7. Thin white lines indicate approximate locations of the orthogonal TEM sections in Figures 3 and 4. **A:** Transverse section (TS) through procarpus (approximately at lowest white line in 3B) where elongated marginal cells *mc1* lie along the apices of three cuticle folds (radii). Each interradial sector of the procarpus is occupied by a pair of cells, the radial cells *pm3*. Cords running longitudinally between the cells of each pair contain nerve dendrites, processes from epithelial cells in the stoma and (in the dorsal cord) the dorsal gland duct (*dgd*). In a few exceptional species including *C. elegans*, the adradial plasma membranec between the cord to the cuticle are missing, however the adradial apical junction (black-bordered red arrows) remains and marks the boundary between the cells. Scale is same as in panel B. **B:** Frontal section through the stoma and procarpus (approximately at the white line in panel A). The basal lamina (*bl*) that envelops the stegostom and pharynx begins anteriorly at *e1*. Red arrowhead, AJs at the boundary between chemoreceptor cells and the sheath cell in the amphid. **C and D:** Left side of the same section of panel B, enlarged to show the boundaries between *hyp1*, *a1*, *a2*, *e1* and *e3*. Note that hemidesmosomes (*hd*) that attach tonofilaments (*tf*) to the cuticle resemble AJs. *sv*, secretory vesicle. The images were modified from unpublished TEMs available from The Worm Image Database (WormImage.org). For details see Methods section.

The differences among taxa in the longitudinal position of cuticular features such as teeth, valves and gland orifices are determined by the lengths

of the different epithelial cell classes. Differences in external shape of the stoma and pharynx are due to differences in diameter and length of the

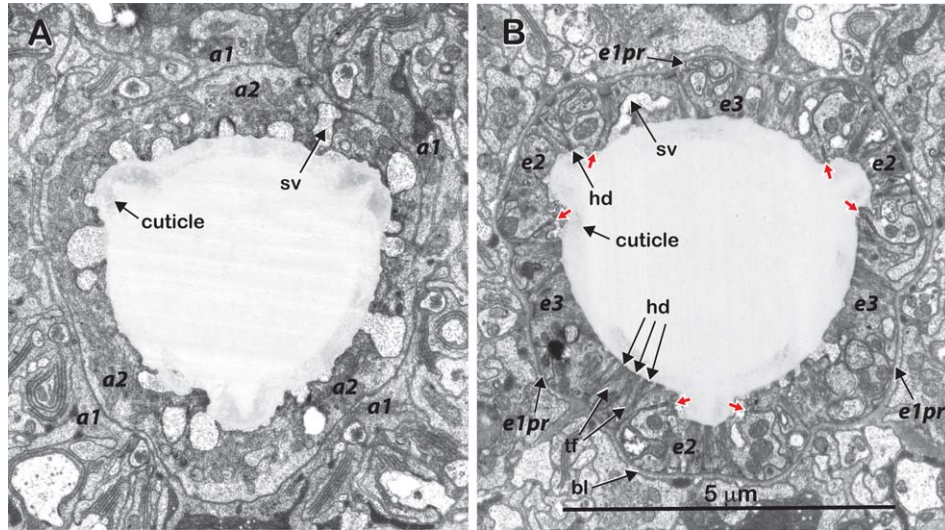


Fig. 4. Features and boundaries of cells surrounding the anterior stoma. For approximate location of sections see Figure 3B, white lines. Secretory vesicles (sv) are involved in the formation of the cuticle, which is faintly visible in these images. **A:** Arcade syncytia *a1* and *a2* of the gymnostom region. This section passes through the toroidal ring of *a2* and processes of *a1* that travel from the more anterior toroid to posterior cell bodies located outside the pharynx. As there are no longitudinal plasma membrane boundaries in each toroid ring, AJs are absent. **B:** Marginal cells *e2* and radial cells *e3* of the anterior stegostom. AJs (red arrows) mark cross-sections of their longitudinal boundaries. The section cuts through processes from *e1*, (*e1pr*), that extend longitudinally past *e3* and connect the more anterior *e1* to its cell body located in *pm3*. The images were modified from TEMs available from The Worm Image Database (WormImage.org). For details see Methods section.

cells (Figs. 2 and 5A). Location of muscular regions is determined as well by which cell classes express muscle cytoskeleton (Fig. 2). In Rhabditida the basic overall shape of the pharynx is expressed as a corpus (often as a separate procorpus and metacorus), isthmus and basal bulb (Fig. 5A). This basic pattern may be further derived within Rhabditida. These shapes are variably found or absent in other taxa; however, the underlying sequence of cell classes in the stoma and pharynx appears to be universal regardless of shaping (De Ley et al., 1995; Ragsdale et al., 2011).

In active pumping regions of the nematode pharynx, the cuticle typically forms three triradiate folds, termed radii, and a row of “marginal cells” lies along each of the radii (Fig. 3A). A row of “radial cells” (syn.: interradii or adradial cells) lies along the sector between marginal cell rows. The radial cells are either single or paired (as for *pm3* of Fig. 3A). Paired radial cells *pm1*–*pm4* are separated by marginal cells *mc1*; paired *pm5* cells are separated by *mc2*. Unpaired radial cells *pm6*–*pm7* are separated by *mc3* in the basal bulb. In *C. elegans* a disc-shaped cell *pm8* caps the posterior end of the pharynx and connects to a pharyngeal-intestinal valve structure.

In all nematodes, a cluster of cell processes, termed a cord (or chord), runs longitudinally through a groove between the paired radial cells (Fig. 3A). Included are thin processes that connect cell specializations located in the stoma with their cell bodies located in the posterior procorpus, as

well as sensory nerve dendrites that lead to the stoma. Each cord also contains a gland duct. The dorsal gland duct *dgd*, is sectioned in Figure 3A as it passes anteriorly through *pm3*. Its opening through the cuticle, the dorsal gland orifice *dgo* (small circle in Fig. 2), is formed by *pm2*. The gland ducts of the subventral cords are not sectioned in Figure 3A as they exit posterior to *pm3*.

In most nematode taxa, the paired radial cell classes *pm1*–*pm5* occur as two distinct cells in each sector that are separated by apposed plasma membranes and a longitudinal AJ (black-bordered red arrows, Fig. 3A), termed “adradial AJ” (De Ley et al., 1995). However, in intermolt stages of a few Rhabditina taxa, including *C. elegans*, the paired cells fuse to the extent that a short segment of apposed plasma membranes that connects between the cord and adradial AJ is missing, as seen in Figure 3A. The separate cytoskeleton and paired-cell topology of *pm1*–*pm5* are nevertheless conserved in these taxa. Because of this, and for the sake of consistency across nematode taxa, we choose to call them “paired radial cells” rather than “syncytia.”

The triradiate cellular architecture of the *mc1* and *pm3* cells of the procorpus (Fig. 3A) is continued anteriorly into the stoma by three rows of the radial cell classes *pm2*, *pm1*, *e3*, and *e1* (Figs. 2 and 3B), which are separated by three rows of the marginal cell class *e2*. Cells *e2* and *e3* are sectioned in Figure 4B. This cellular architecture is observed in all taxa investigated so far by TEMs

(Fig. 1). In most nematode taxa including the three illustrated in Figure 2, the Y-shaped lumen of the procorpus morphs through a triangular shape in the *pm2* and *pm1* regions and into the nearly cylindrical form of the *e3*, *e1*, *a1*, and *a2* regions. The three *e2* marginal cells maintain shallow grooves in the otherwise smooth cuticle

lining (Fig. 4B). We reclassify *e2* as a marginal cell instead of “epithelial cell” (Albertson and Thomson, 1976) because it is identical in function and form to marginal cells *mc1-mc3*.

In all taxa, the radial cells *pm1* and *pm2* resemble *pm3* in consisting of 3 sets of paired cells separated by a cord and a longitudinal adradial AJ. For each of these cells, the anterior specialized region is separately connected posteriorly by a thin process to its cell body and nucleus located in the procorpus. Thus there are six nuclei associated with each of the paired radial cell classes *pm1* and *pm2*. Radial cells *e1* and *e3*, on the other hand, exist as only one cell per interradiial sector with no cords or adradial AJ (Fig. 4B). The posterior process from the specialized region of each of these connects posteriorly to its cell body and one nucleus, thus there are three nuclei associated with each of the unpaired radial cell classes *e1* and *e3*.

The unusual fusion in *C. elegans* of the anterior muscular segments of the six *pm1* cells into one circumferential muscle (still connected by

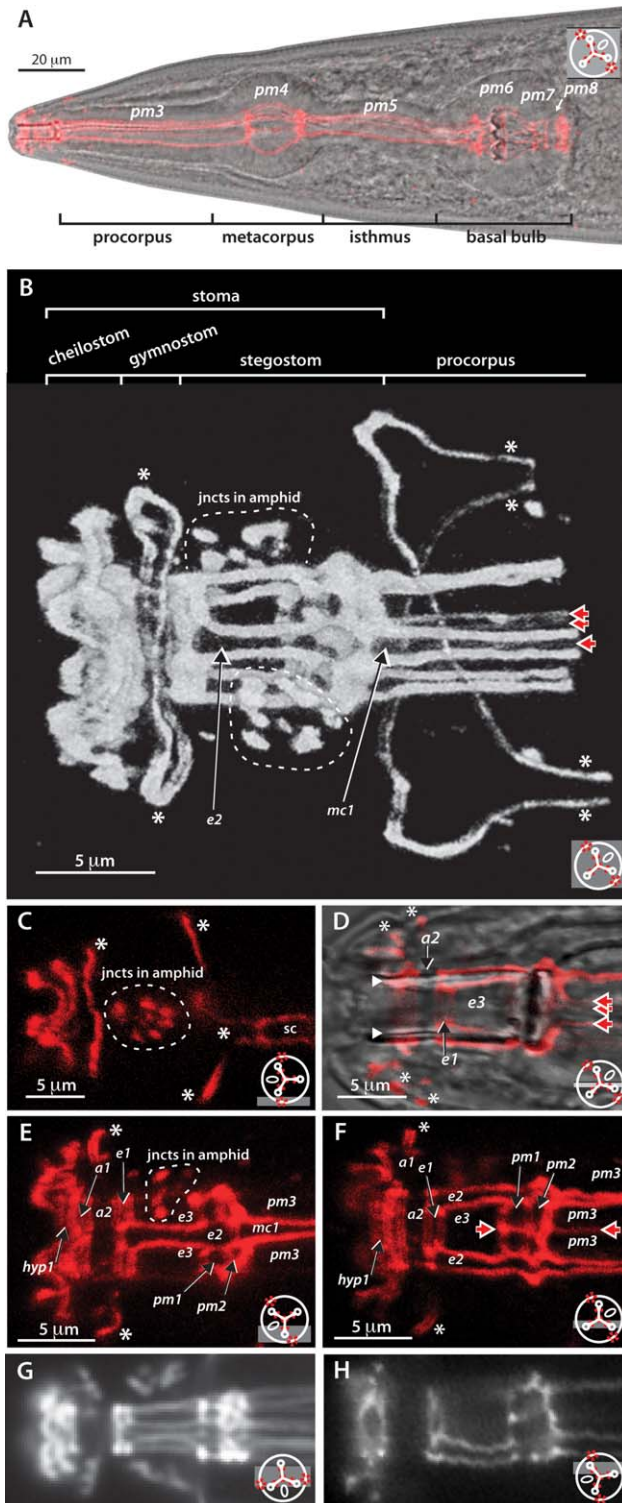


Fig. 5. Confocal microscopy of fluorescent MH27 antibody-labeled apical junctions in the anterior of *C. elegans*. AJs appear as fluorescent ribbons along the luminal cuticle. These mark the longitudinal and circumferential boundaries of the pharyngeal epithelial cells. Images were prepared from a multifocal series of optical sections consisting of fluorescent images and, in the same focal planes, DIC images. See supplementary online material text-S2 for details. *Circular diagrams* at lower right of each panel indicate orientation of the specimen and sections in the voxel array. The oval (representing the dorsal gland duct) indicates the dorsal sector, the horizontal gray band indicates depth and thickness of the selected slab of voxels, red marks indicate the location of AJs, and dashed red lines encircle apical junctions in the amphids. In the images, *white-bordered red arrows* at right point to the longitudinal ribbons of the adradial AJs, the \* indicate hypodermal cell boundaries at the body cuticle and dashed white lines encircle apical junctions in the amphids. Specimens were *C. elegans* adult hermaphrodites except those of C and G, which were J3 juveniles. **A**: Entire pharynx. Composite of fluorescent and DIC images, left subdorsal view. A slab of 40 fluorescent optical sections (8  $\mu$ m) that include just the pharynx, was projected then merged with a median DIC optical section from the same multifocal series. See supplementary online material video-V1 for a through-focus movie of the original image array. **B**: Stoma and procorpus. Volume-rendered 3D visualization of a 20  $\mu$ m slab of 100 fluorescent optical sections. For original array see Supplementary online material video-V2. **C**: Left amphid, lateral view. *sc*, seam cell along the lateral body cuticle. Eleven optical sections (1.6  $\mu$ m slab) were averaged. **D**: Adjacency of apical junctions and stoma cuticle (*white arrowheads*). Composite of fluorescent and DIC images from a 1.0  $\mu$ m slab near the median plane. (Supplementary online material video-V2). **E**, **F**: Precisely oriented views of an expanded voxel array. Voxels were made equidimensional by increasing the number of images in the *z* dimension. **E**: Left subdorsal row of marginal cells *e2* and *mc1* (3.4  $\mu$ m slab, averaged). **F**: Right subventral row of radial cells (1.6  $\mu$ m slab, averaged). **G**, **H**: Equivalent views of specimens by epifluorescence microscopy. A single optical section was obtained in specimens with different orientations. ‘Section thickness’ is predetermined by the depth of focus of the microscope optics. The gray band in the circular diagrams was estimated from the appearance of structures in the image.

processes to six posterior cell bodies) appears to be a derived character.

The cells lining the stoma and pharynx, in addition to functioning as epithelial cells interfacing between the body extracellular compartment (pseudocoelom) and the lumen (Michaux et al., 2001), may or may not be expressed as muscles. In most nematode taxa, including *Zeldia*, radial cells *e1* and *e3* express muscle, while in a few others, for example, *Caenorhabditis* and *Bunonema*, they do not (Fig. 2). Therefore, it is inappropriate to distinguish *e1* and *e3* as “epithelial cells” while calling the other radial cells “muscle cells.” We argue for using topological terms “unpaired radial cells” instead to differentiate cell classes *e1*, *e3*, and *pm6-7* from the “paired radial cell” classes (see Discussion section).

### Observation of Cell Boundaries by Immunofluorescence and the Confocal Microscope

Apical junctions (AJs) are identifiable in TEMs as densely-staining thickenings of the plasma membranes (red arrows in Figs. 3 and 4B). These run from the cuticle inwardly for a short distance along the plasma membranes of adjacent epithelial cells and thus form a narrow belt or ribbon around each cell at the border between cells. Only cross sections through these borders are visible in TEMs and reconstruction from serial sections is necessary to visualize the cell boundaries.

With the AJs rendered fluorescent by binding MH27-IgG-Cy3, the boundaries of epithelial cells appear as bright fluorescent ribbons that lie adjacent to the lumen cuticle (Fig. 5). The MH27 antibody specificity for AJs identifies them unambiguously. The cylinder of longitudinal ribbons seen in Figure 5A,B consists of the longitudinal boundaries; circumferential ribbons intersecting the longitudinal ribbons are the anterior-posterior boundaries.

Fluorescence images obtained by the epifluorescence microscope (Shakes et al., 2012) provide useful information about the cellular architecture (Fig. 5G,H); however, confocal images of the same region (Fig. 5E,F) have better resolution and contrast (White et al., 1987). Another advantage is that the confocal microscope digitizes a series of optical sections at accurately spaced intervals through the specimen, thus recording morphology in three dimensions. For an example see the through-focus supplementary online material video-V2. With the 63 $\times$  objective the axial resolution provided noticeably different adjacent sections at 0.16 or 0.2  $\mu\text{m}$  intervals. As well as the confocal fluorescence image, an image of transmitted light for comparison was recorded at each focal plane with optics set for either bright-field or DIC-illumination.

Image processing software packages such as ImageJ treat the stack of fluorescence images as a 3D array of “voxels,” with *x* and *y* dimensions equal to the spacing between pixels in the images and *z* dimension equal to the spacing between the optical sections. Slabs, consisting of a number of optical sections, were selected and projected onto a plane parallel to the slab by computing either the average or maximum intensity in each column of voxels. For the 3D visualization in Figure 5B, a volume rendered image was computed from the selected slab using Image Surfer 2 (Feng et al., 2007). In order to provide a favorable view of a specific region as in Figure 5C,E,F, the voxel array was rotated before selecting the slab. However, before rotating, the voxel *z* dimension, initially the spacing between optical sections, had to be made the same as the pixel *x* and *y* dimensions by expanding the voxel array. For details see supplementary online material text-S2.

Figure 6 illustrates both longitudinal and transverse sections at different locations in an array of equidimensional voxels. Each transverse section (TS) of Figure 6D–I was prepared by selecting the longitudinal region of interest in the longitudinal sections (LSs) of the voxel array and projecting it onto a plane perpendicular to the body axis. A series of TS was thus prepared at an *accurately* determined longitudinal position in LSs of the *same* specimen. The dimensions through the specimen are exactly known from the voxel dimensions provided by the application software for the confocal microscope (see scale bars).

The *yz* plane of TS images (Fig. 6D–I) reveals a physical characteristic of confocal microscopy. The streaking of fluorescent spots parallel to the optic axis originates from diffraction of the light emitted by each point fluorescent source (Cy3-conjugate of the secondary antibody) in the specimen. The design of confocal optics eliminates much of the blurring in planes perpendicular to the optic axis, greatly improving resolution in the *xy* dimension; however, it cannot decrease the axial blurring that causes the narrowed streaks. The axial blurring in the voxel array can be minimized post hoc by deconvolution algorithms; however, deconvolution did little to improve our images. To be effective the algorithms usually require a prior run on reference particles in the microscope to determine a point spread function for its optics (Sibarita, 2005).

The TS images are useful for observing changes in the shape of the lumen cuticle along the stoma, since the AJs lie along the cuticle. For example, comparison of Figure 6I, a TS through *pm3* and *mc1*, with Figure 6H through *pm1* and *e2*, reveals that the three adradial AJs (black-bordered red arrows) move from a position medial to the six marginal junctions along the cuticular radii to a position equiradial to the marginal junctions. This

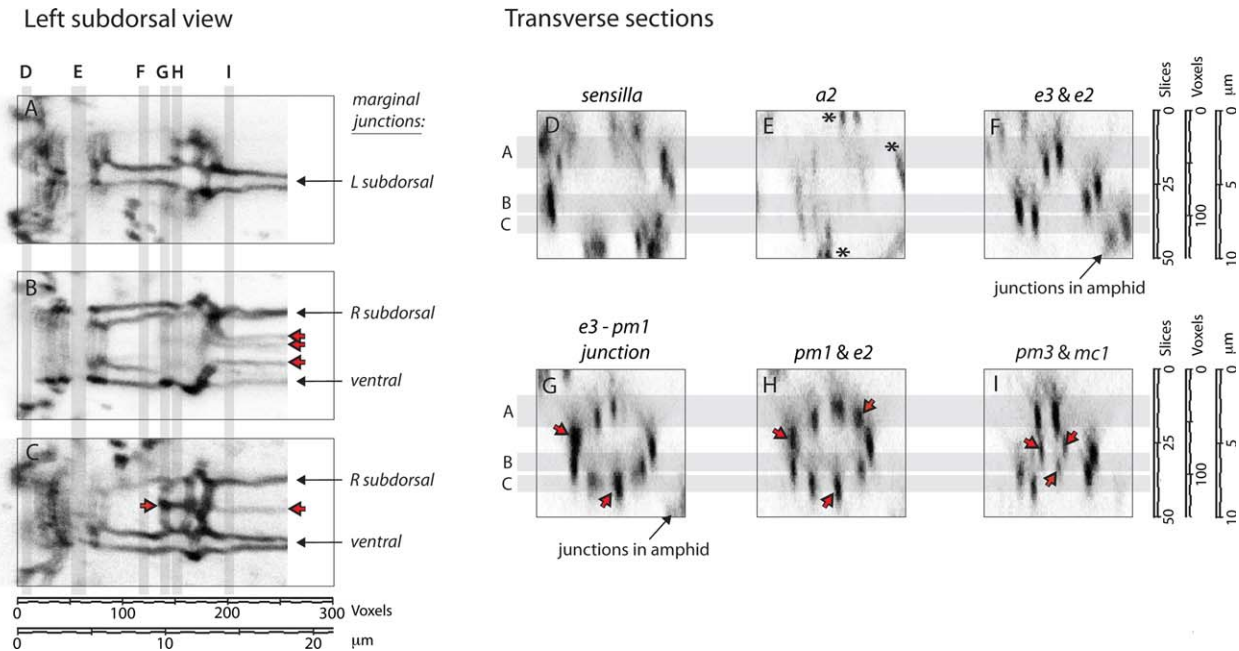


Fig. 6. Apical junctions in accurately related LSs and TSs through the same *C. elegans* hermaphrodite. Location and thickness of each section is indicated by the grayed bands on the orthogonal sections. See scales at bottom and right. **A–C: Longitudinal sections.** Adradial AJs are marked by black-bordered red arrows. (See the original image array in Supplementary online material video-V2) **D–I: Transverse sections:** The equidimensional voxel array was rotated to a rear-on view before selecting transverse slabs (See methods in Supplementary online material text-S2; resulting array in Supplementary online material video-V3). View is looking anteriorly along the body axis; dorsal toward upper right. Cross-sectioned longitudinal boundaries in the stoma and procorpus appear as a hexagonal array of fluorescent spots (distorted by the lower resolution along the optic axis). Labels at the top of each panel indicate the cells that the TS passes through. The hypodermal cell AJs (\*) that line the body cuticle are seen in E but lie outside the same space in F–I because the body is wider. Black-bordered red arrows mark the three adradial AJs that are sectioned in G, H and I. It is clear from the longitudinal and transverse sections that these change from low density in *pm3* to a higher density in *pm2* and *pm1* and do not continue into *e3* and *e1*. In the section that borders *pm1* and *e3* (panel G), the dorsal adradial AJ is not included (space in upper right) as that corner of the section passes through *e3*. Also the extra density of the ventrolateral adradial AJs in this section is probably due to the junction of the sensory nerves *I2* with the cuticle (See Fig. 8, 300° and 60° rotations).

corresponds to a transition from a deep position on the Y-shaped folded cuticle of *pm3* (Fig. 3A) to the more peripheral position on the cylindrical cuticle that begins in *pm2* and continues through the stegostom (Fig. 4B). In every TS posterior to *a2* (Fig. 6F–I), the cross-sectioned longitudinal junctions provide nine fiducial points that can be used for accurately mapping the cuticular lumen as it changes.

### Identifying Cellular Architecture

With an understanding of the distinguishing features and arrangement of the cell classes, one can usually identify the stoma cell boundaries without the aid of TEMs. The three prominent pairs of longitudinal ribbons seen in Figure 5B are the longitudinal boundaries of marginal cells with radial cells. Their adjacency to the refractile cuticle becomes evident in merged fluorescence and bright-field images such as Figure 5D. The sections of Figure 5E,F are through the same voxel array that had been rotated to provide favorable views (note the orientations indicated by the circular diagrams).

Central in Figure 5E are the longitudinal boundaries between a row of marginal cells (*e2* and *mc1*) and two rows of radial cells (*e1*, *e3*, *pm1*, *pm2*, and *pm3*). In Figure 5F two marginal cell rows are seen on either side of a radial cell row. Anterior-posterior boundaries are clearly observable: between marginal cells *e2* and *mc1* in Figure 5E,B, and between radial cells in Figure 5F.

Of special interest with regard to the well-described pharynx of *C. elegans* (Albertson and Thomson, 1976), our confocal images reveal that marginal cells *e2* and *mc1* are adjacent, with a single circumferential (anterior–posterior) boundary between them and with continuous longitudinal boundaries along the radial cells. This is a new finding. The reconstruction from serial TEM TSs, on which the WormAtlas (Altun and Hall, 2009) is based, concluded that *e2* and *mc1* are separated longitudinally by a circumferential extension of *pm1* (Albertson and Thomson, 1976). This is clearly controverted by the confocal sections (Figures 5 and 6). That the *pm1* cells interconnect peripheral to the continuous *e2* rows will be shown in TEMs in a subsequent article.

Three other longitudinal ribbons (white-bordered red arrows) occur in the stoma and pharynx—three are seen in the medial section of Figure 5D, one in the off-medial section of Figure 5F and three are exposed beside and between the pair of marginal junctions in Figure 5B. These are the adradial AJs seen sectioned in TEM TSs (Fig. 3A, black-bordered red arrows) and they mark the longitudinal boundary dividing radial cell pairs *pm1*, *pm2*, and *pm3*. In Figure 5F this boundary is clearly continuous through this region and does not extend anterior to the paired cells into the region of single, unpaired cells *e3* and *e1*. This pattern is diagnostic for the paired and unpaired radial cell classes.

The circumferential borders of *e1* and *a2* are distinct and the borders of the very thin cells *a1* and *hyp1* can be distinguished in Figures 5E–H and 6A,C. The bright ribbons along the longitudinal AJs terminate abruptly at the *e1/a2* border (Fig. 5B,D–H). This corresponds to the termination of the marginal cell rows and the absence of longitudinal plasma membranes dividing the toroidal syncytia *a1* and *a2* (Fig. 4A). The change is also noticeable between transverse sections through the *e3* and *e2* region (Fig. 6F) and the *a2* region (Fig. 6E) of the voxel array.

In the low magnification composite image of Figure 5A, the circumferential borders between *pm3*, *pm4*, *pm5*, and *pm6* can be located within the metacarpus, isthmus and anterior basal bulb. A higher magnification confocal series would be needed to unravel the complex architecture in the basal bulb, where *pm6–8* occur and where, in some species including *C. elegans* and *Z. punctata*, the luminal cuticle morphs into the grinder (Zhang and Baldwin, 2000, 2001; Altun and Hall, 2009 PhAFIG 8B).

Thus, in the voxel array provided by the confocal microscope, one can readily locate the cell classes lining the luminal cuticle from the stoma to the basal bulb. In the pattern of fluorescent ribbons the paired radial cells *pm1–5*, the unpaired cells *e1*, *e3*, *pm6–7*, and the toroidal cells *a1*, *a2* are readily differentiated.

### Application to Other Nematode Species

Fluorescence and DIC images at three depths in *Zeldia punctata* and *Bunonema* sp. are compared in Figure 7 with equivalent images of *C. elegans*. The views (orientations) of the three specimens are geometrically equivalent with respect to the triradial symmetry—the upper, medial, and deeper sections through the specimens include equivalent boundaries. For *C. elegans* and *Z. punctata*, the patterns of cell classes are clearest. Longitudinal ribbons occur in *Z. punctata* as in *C. elegans* with a gap next to the cheilostom that identifies the gymnostom. Circumferential ribbons

identifying the boundaries between *hyp1*, *a1*, and *a2* are distinguishable at the three depths.

In the deepest sections (bottom row of Fig. 7) the continuous longitudinal ribbon passing through the center of a radial cell row is the adradial AJ and identifies the paired *pm1*, *pm2*, and *pm3*. The two radial cells anterior to these lack the adradial AJ, and therefore must be *e3* and *e1*. Cells *e1* and *pm2* are proportionately much longer in *Z. punctata* than in *C. elegans*. This is comparable to observations from TEMs (Fig. 2). In the upper sections of *Z. punctata* and *C. elegans* (top row of Fig. 7), a circumferential ribbon crossing the marginal cell row identifies the boundary between *e2* and *mc1*.

The brighter fluorescing dots along the longitudinal junctions of *e1* and *e3* are end-on views of circumferential ribbons where they travel along the optic (*z*) axis. These should be distinguished from the spots in the junctions bordering *pm1* and *pm2* in *C. elegans* and *Zeldia*, where the circumferential ribbons intersect with the adradial AJs. These spots are due to the larger mass of AJs where sensory nerve processes or the *dgo* contact the cuticle. The locations of these regions around the lumen are more accurately illustrated in the cylindrical projections of Figure 8. In the left subdorsal views of Figure 7, the junctions of *I2* and *I1* are recognized along the central adradial AJ of deeper sections of *C. elegans* and at least one junction in *Zeldia* (See pattern at 300° rotations in Fig. 8). In the middle section in *C. elegans* (Fig. 7), the contacts of *I3* and the *dgo* with the cuticle can be seen as spots along the left adradial AJ.

Images of the much thinner *Bunonema* sp. include the entire body width. The outer ribbons, adjacent to the body cuticle, identify boundaries between hypodermal cells (asterisks). The dense spot at the anterior end of the hypodermal boundaries is probably a cross-sectioned circumferential boundary. The more medial longitudinal ribbons lie along the stoma cuticle. The patterns at the three depths resemble those of *C. elegans* and *Z. punctata* and the longitudinal boundaries of the radial and marginal cells are evident. At least two of the adradial AJs can be discerned in the procorpus (median and deeper sections), where *pm3* cell pairs are expected. A region of dense spots anterior to *pm3* resembles the *pm1* and *pm2* regions in *C. elegans*, but it is more compressed longitudinally. The extensive region anterior to *e1* lacks longitudinal boundaries (rows of spots), consistent with the observation from TEMs (Fig. 2) that the arcade cells *a1* and *a2* of the gymnostom are unusually long in *Bunonema* sp. The distance between the *a2–e1* and *pm2–pm3* borders is about 2  $\mu\text{m}$  and the borders between *e1*, *e3*, *pm1*, and *pm2* are unresolved. In TEMs these cells appear to be approximately 0.3, 0.4, 0.8, and 0.3  $\mu\text{m}$  thick, respectively (Dolinski and Baldwin, 2003). The

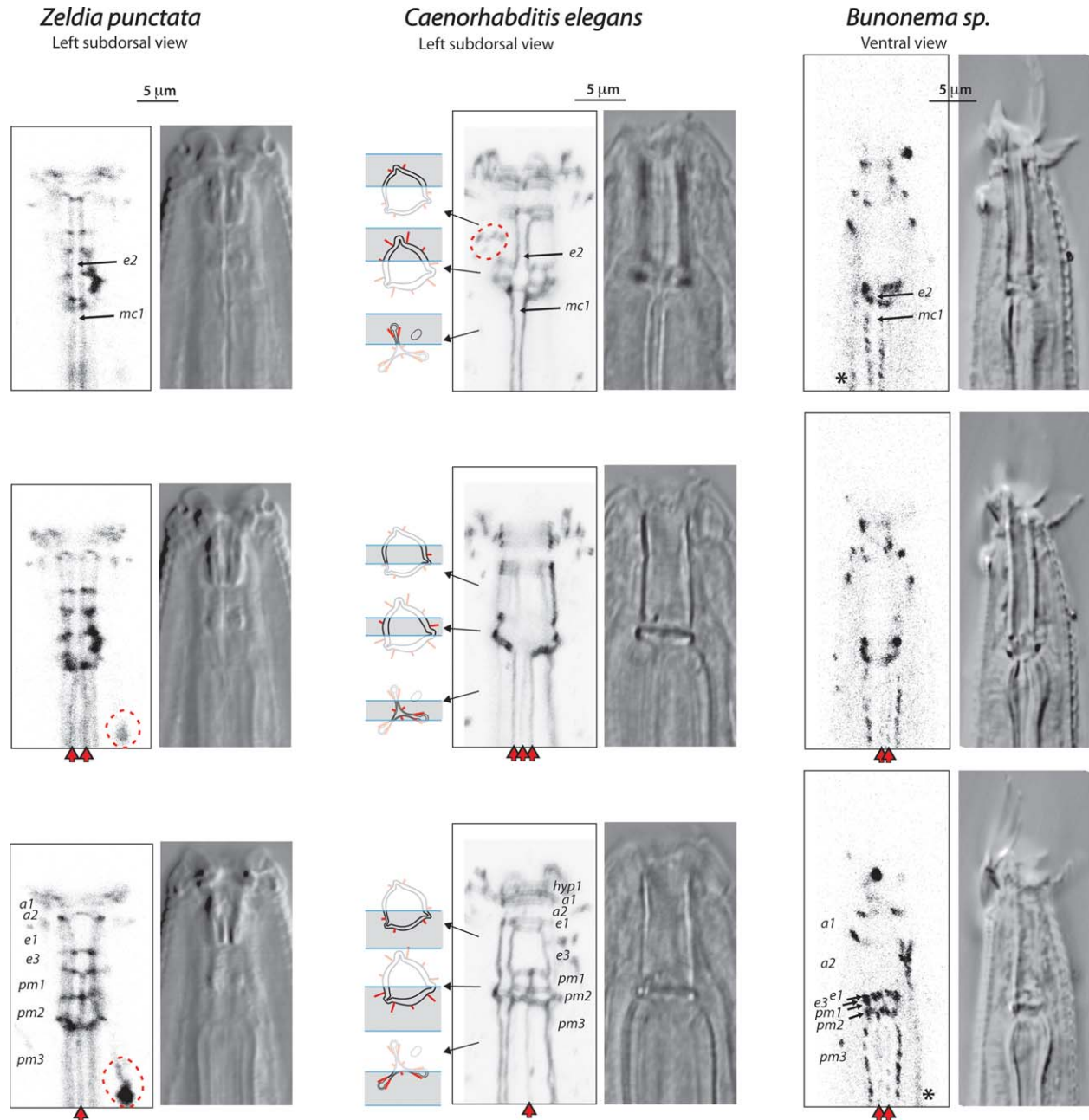


Fig. 7. Evidence of homology of cellular architecture in *Zeldia punctata*, *C. elegans* and *Bunonema* sp. Longitudinal sections at three depths were chosen to contain equivalent structures in each species. Marginal cells are labeled in the first row; radial cells in the third row. *Black-bordered red arrows* point to adradial AJs in *pm1-3*. The \* in *Bunonema* images identify hypodermal cells lining body cuticle. *Circular diagrams* (from TSSs of *C. elegans*) indicate the structures and apical junctions (red marks) that are intercepted in three longitudinal regions of each section: the *e2-e3*, *e2-pm1* and *mc1-pm3* regions. Grayed areas indicate thickness and depth of each section. For original arrays see Supplementary online material video-V2, video-V4 and video-V5.

locations of the unresolved cells are suggested by the labeling in the lowest image of Figure 7 and by the broken lines in Figure 8. In the images of *C. elegans*, the technique resolves the 1.0  $\mu\text{m}$ -spaced boundaries of *pm2* and 0.75  $\mu\text{m}$ -spaced boundaries of *e1*.

All of the longitudinal ribbons in the stoma and procorpus of *Bunonema* occur as a row of spots (as

if the MH27 epitope were discontinuous along the cell boundaries). This was observed in all three specimens of *Bunonema*. Of interest, such punctate staining has been observed transiently during formation of epithelial ribbons during morphogenesis in *C. elegans* embryos (Bossinger et al., 2001; Portereiko et al., 2004). It is curious that mature ribbons are not formed in *Bunonema* sp.

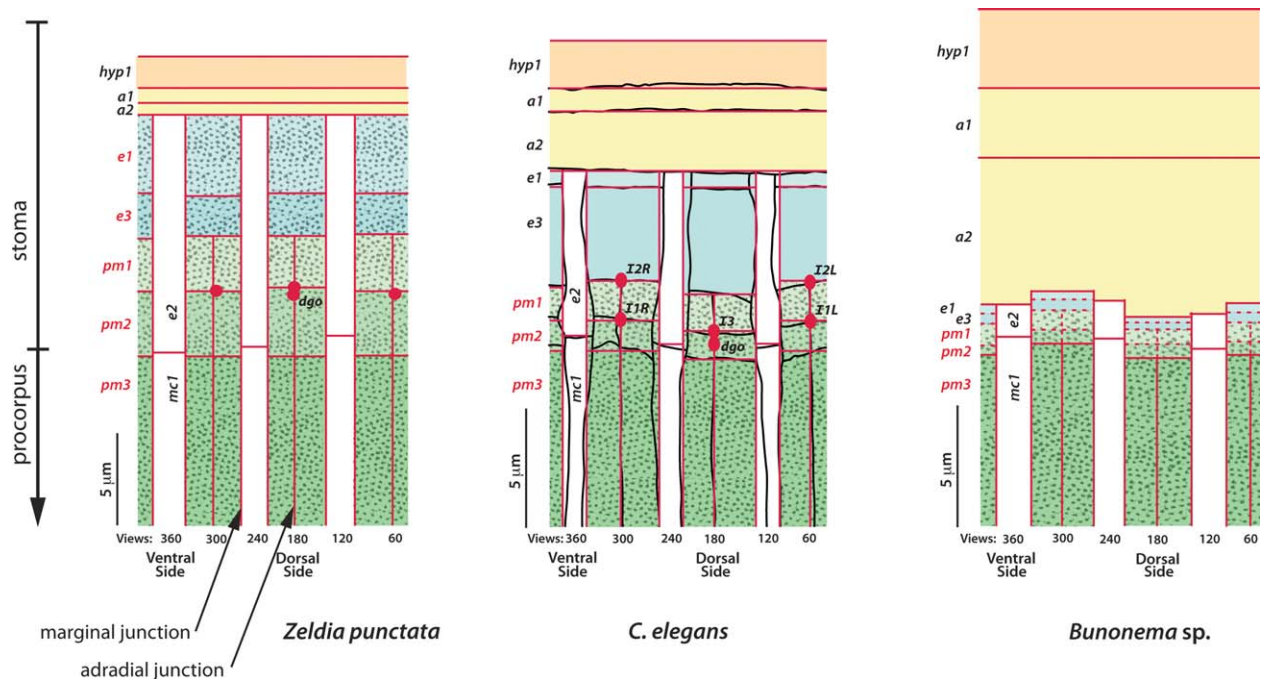


Fig. 8. Cylindrical projections of cellular architecture along the stoma cuticle. Red lines indicate location of fluorescent cell boundaries. Large red dots represent the bright fluorescence originating from denser apical junctions surrounding the dorsal gland duct orifice (*dgo*) and around nerve processes (*I1*, *I2*, *I3* in *C. elegans*) where they contact the stoma cuticle. The colored areas identify cell classes as in Figure 2. The underlying dotted pattern and red labeling indicates the radial cell classes that express muscle in each species. *Dorsal side* and *Ventral side* indicate the side of the lumen where the apical junctions are located. Dotted red lines in *Bunonema* sp. represent junctions between closely-spaced radial cells that are unresolved in the confocal microscope but are confirmed in TEMs (Fig. 2). Slabs of images that include the fluorescent ribbons on the far side of the lumen cuticle, as in Figure 5E,F and in the third row of Figure 7, were selected from equidimensional voxel arrays that had been rotated by 60° increments. Longitudinal and circumferential fluorescent boundaries in the projected images were traced in Adobe Illustrator, adjoining the tracings to produce the cylindrical projection. For details see Supplementary online material text-S2. Black lines in *C. elegans* are the actual tracings. Red straight lines in each species are approximations made for simplicity.

Bright fluorescent spots mark the amphids in the three species. Whereas in *C. elegans* the labeled AJs are located lateral to the *e2* region, the amphid AJs of *Zeldia* are located posterior to the stegostom (Fig. 7, dashed red lines), and those of the single amphid of *Bunonema*, not visible in these sections, occur near the *a1-hyp1* boundary. The two large bright spots in the tip of *Bunonema*, visible in the upper and lower sections, are located at the base of papillae and probably mark AJs associated with sensory dendrites in contact with or passing through an epithelial boundary, as for amphidial AJs.

The architecture along the lumen cuticle of the three species could be investigated in greater detail by projecting a series of slabs through the far side of the lumen at successive 60° rotations of the voxel array. Figure 8 summarizes the observations as a cylindrical projection. The sequence of cell classes along the stoma is the same in the three species although their longitudinal extent varies. Adradial AJs are observed in *pm1*, *pm2*, and *pm3* but not in the single unpaired radial cells *e1* and *e3*. In the images of *C. elegans* and *Zeldia*, a brighter fluorescence (red dots) mark where the

dorsal gland orifice (*dgo*) passes through the dorsal cuticle and where sensory nerve processes contact the cuticle. These locations are consistent with those illustrated in TEM reconstructions of *C. elegans* (Albertson and Thomson, 1976), and of a species closely related to *Zeldia punctata*, *Acrobeloides* sp. (De Ley et al., 1995).

## DISCUSSION

### Previous Application of Fluorescent MH27 and Confocal Microscope

The Brenner lab using TEM reconstructions and Nomarski (DIC) optics laid the foundations for *C. elegans* research (see Sulston et al., 1983 for references), but also revealed a need for a rapid, high-contrast method for observing cell boundaries. White et al. (1987) developed the laser scanning confocal microscope for greatly improved resolution of immunofluorescence-stained components of cells, and Podbilewicz and White (1994) first applied the MH27 antibody for fluorescence-staining of epithelial cell boundaries. They used it with confocal microscopy to investigate the disappearance of AJs during hypodermal cell fusions

that occur during embryonic development. With the introduction of GFP constructs (Chalfie et al., 1994) and germline transformation techniques (Mello et al., 1991), the expressed reporter gene construct AJM-1::GFP (originally called JAM-1::GFP) has become the method of choice for marking the AJs in *C. elegans* (reviewed by Simske and Hardin, 2001; Hutter, 2012); however, this approach cannot be applied to other taxa with current technology.

Shemer et al. (2004; reviewed by Podbilewicz, 2006) used AJM-1::GFP recombinants, time-lapse confocal microscopy and heat-shock-initiated expression to show that the membrane protein EFF-1 controls hypodermal cell fusion during morphogenesis. Fusion of radial cell pairs, which occur in *C. elegans* at about the time of hatching (Sulston et al., 1983), cannot be observed by fluorescence-labeling AJs because the AJs do not disappear after fusion of these cells. Instead, Shemer et al. (2004) used TEM serial sectioning and heat-shock-initiated expression in *eff-1(-)* mutants to show that EFF-1 is necessary for fusion in radial cell pairs. Of considerable interest in this regard, fusion of radial cell pairs is known to occur in Nematoda only in Rhabditina, and within that suborder only in the Eurhabditis clade within Rhabditomorpha and in Diplogasteromorpha (Fig. 1). Expression of EFF-1 in radial cell pairs thus would appear to be an evolutionarily derived trait.

## Extensions for Investigating Nematode Stoma

The stoma was not covered in the classical work on morphogenesis in *C. elegans* (Sulston and Horvitz, 1977; Sulston et al., 1983), and subsequent work to date has been on the arcade cells (Mango, 2007, 2009; Portereiko and Mango, 2001; Portereiko et al., 2004) in one lab, and *pm8* and cells forming the pharyngeal-intestinal valve in another (Rasmussen et al., 2008, 2012, 2013). Marginal and radial cell classes have yet to be investigated. In this article we apply MH27 and confocal microscopy to describe the entire *C. elegans* stoma and find that the continuity and extent of cell boundaries are shown to a degree not achievable in ultrathin sections for TEM. In the patterns of fluorescent ribbons one can distinguish among the hypodermal and arcade cells, marginal cells, and both single and paired radial cells. The power of the technique is underlined by our discovery of a feature that had not been noticed in a TEM reconstruction of the *C. elegans* pharynx (Albertson and Thomson, 1976): that *e2* and *mc1* share a circumferential border at the cuticle, and thus the row of marginal cells is continuous as in other nematodes.

One main objective of this research was to provide a tool for investigating cellular architecture

in diverse nematode taxa that is not as limited by cost and time as with reconstruction from serial sections and TEM (e.g., Bumbarger et al., 2006, 2007; Ragsdale et al., 2011). We show here that the *C. elegans* monoclonal antibody MH27 also binds specifically to AJs in *Zeldia punctata* and *Bunonema* sp. It had been previously applied to nine species closely related to *C. elegans* (Fitch and Emmons, 1995) and *Pristionchus pacificus* (Kolotuev and Podbilewicz, 2004). With *Zeldia* we extend its application to a more distant suborder of Rhabditida, Tylenchina (Fig. 1). As the molecular divergence within the Eurhabditis clade within Rhabditomorpha is at least as great as that between mouse and sea urchin (Kiontke and Fitch, 2005), the *C. elegans* antibody MH27 appears to cross-react with a relatively wide range of taxa. It has yet to be tried on more distant taxa.

Starting with fluorescent-stained whole mounts, a multifocal stack of high contrast optical sections of the network of cell boundaries is obtained in minutes by the confocal microscope, and is readily processed with free-access software to provide either two-dimensional (2D) sections or 3D-visualizations (e.g., Fig. 5). As detailed in the Results, section orientation, thickness and depth can be chosen post hoc. Borders spaced 0.75  $\mu\text{m}$  apart are resolved. One can readily differentiate among the toroidal, unpaired and paired architectures of the cell classes. Both TSs and LSs can be made of the same whole mount at accurately selected locations. In TSs, the cross-sectioned longitudinal fluorescent ribbons provide fiducial marks useful for mapping changes in shape of the luminal cuticle in a series of TSs. A cylindrical projection of cellular architecture can be traced from images obtained at successive rotations of the voxel array, in which the dorsal gland orifice (*dgo*) and sensory nerve processes can be located relative to the cell boundaries. Fluorescent labeling with MH27 also provides good evidence for the absence of cell boundaries, useful for recognizing the *a1*, *a2*, *e1*, and *e3* cell classes, or the disappearance of adradial AJs during fusion of the hypodermal cells (Podbilewicz and White, 1994).

## Homology of Cell Classes

The patterns of fluorescent ribbons show that the sequence of cell classes is the same in the three taxa investigated (Figs. 7 and 8). A survey of all TEM level descriptions of the stoma and procorpus (Fig. 1) extended the review by De Ley et al. (1995) to include most of the major phylogenetic clades of nematodes. The same pattern of cell classes is recognizable and the distinction between the single *e1* and *e3* cells and paired *pm1-pm3* cells is maintained in all the taxa even though other features of stoma morphology and function may vary. However, in only the

Rhabditida has there been an adequate sampling of the taxon by TEM; in most orders there are only one or two examples and for two major groups, the Chromadorida and Desmodorida, there are none (Fig. 1).

We have dealt with an apparent exception in *C. elegans* stoma. Albertson and Thomson (1976) observed that the six *pm1* cells fuse to form a circumferential muscle; however, they illustrated the toroidal structure as a single toroidal cell process passing between *e2* and *mc1*, thus interrupting the continuity of the marginal cell row. We show here that this currently accepted morphology (Altun and Hall, 2009) is incorrect. Fluorescent antibody-labeled AJs (Figs. 5 and 8) show clearly that the *pm1* cell boundaries do not cross the longitudinal boundaries along the marginal cell row and that *e2* and *mc1* are adjacent in the marginal cell row. In a forthcoming article we will show with TEMs that the connecting circumferential processes pass peripheral to the junction. Interestingly, circumferential muscles occur also in *pm8* of *C. elegans* and sporadically in other taxa, for example, in *e1* of *Zeldia*, *pm1* of *Aphelenchus avenae* and *pm3* of tylenchids *sensu stricto* (Ragsdale et al., 2011). Thus a circumferential muscle in the stoma or pharynx appears to be a derived character, probably to provide a constraining or sphincter function to certain regions of the pharyngeal tube.

Whether a cell class expresses muscle cytoskeleton or not depends on the taxon (De Ley et al., 1995; Ragsdale et al., 2011). In view of this diversity in expression of muscle in the otherwise homologous cell classes and to provide a consistent terminology that applies to the architecture across taxa, we propose that functional descriptors (muscle, epithelial, syncytial) for the different cell classes be replaced by topological ones (toroidal, marginal, radial, paired, unpaired). It is confusing to distinguish *e1* and *e3* in *C. elegans* from so-called muscle cells by calling them “epithelial cells” while in most other nematodes *e1* and *e3* are muscles. While they are non-muscular in the Rhabditina, they are muscular in all taxa in the sister suborder Tylenchina with only one apparent exception: in *Aphelenchus avenae* *e3* is clearly non-muscular, while *e1* has both extensive muscular and non-muscular regions (Ragsdale et al., 2011). So-called muscle cells *pm1-5* are muscle in most taxa with the exception that *pm1* and *pm2* do not express sarcomeres in the tylenchids *sensu stricto* (Baldwin et al., 2004; Ragsdale et al., 2011) and *pm3* is non-muscular in *Trichodorus* (Triplonchida), which has independently evolved a modified tooth analogous to the stylet of other plant parasites (Hirumi et al., 1968; Raski et al., 1969). Interestingly, marginal cells *e2* and *mc1* are non-muscular in most taxa; however, they express muscle cytoskeleton in Mononchida and Dorylaimida (Grootaert and Coomans, 1980).

The cellular architecture posterior to the procorpus has not been as widely investigated as in the stoma and proximal procorpus, and confocal microscopy has great potential for investigating the clearly outlined cell boundaries in this region (Fig. 5A). At least within Rhabditida there is some TEM-based support for a conserved sequence of homologous cell classes posterior to the procorpus. In *C. elegans*, the triradiate architecture of marginal and radial cells continues as *mc1* associated with *pm1-4* in the stegostom and metacarpus, *mc2* with *pm5* in the isthmus, and *mc3* with *pm6-7* in the basal bulb (Albertson and Thomson, 1976; PhaFIG 6, WormAtlas). While *pm1-5* are paired, each of the three *pm6* and *pm7* cells contains a single nucleus and they are unpaired like radial cell classes *e1* and *e3*. The disk-shaped toroidal cell *pm8* caps the posterior end of the pharynx and connects the cuticular lumen to the pharyngeal-intestinal valve structure.

This same posterior architecture is found in *Zeldia punctata* and *Teratocephalus lirellus* (Zhang and Baldwin, 2000, 2001). Like *C. elegans*, these are bacterial feeders that have a grinder, an elaborate cuticular structure in the basal bulb that is associated with, and probably formed and operated by *pm6-7*. A grinder is not found outside of Rhabditida and would be characteristic of that order except that it appears to have been lost in separated clades within that order including: Diplogasteromorpha and Tylenchomorpha (Fig. 1). Therefore two observations in these suborders are especially interesting. In *Diplenteron* sp. (Diplogasteromorpha), along with the grinder, one of the unpaired, grinder-associate classes *pm6-7* is absent as well as the toroidal *pm8*. On the other hand, in *Basiria* (basal in the Tylenchomorpha phylogeny), the *pm6-7* are retained for an apparent pumping role (Baldwin et al., 2001). Otherwise, the sequence of marginal and radial cell classes is identical to that of the bacterial feeders (Zhang and Baldwin, 1999). As in the posterior pharynx, one might expect to find examples in the stomal region where the basal template of cell classes is altered by deletions; however, none has been discovered so far (Fig. 1).

Also interesting, in the stylet-bearing pharynges of the putatively more derived Tylenchomorpha and tylenchids *sensu stricto*, all cell classes posterior to the isthmus cells *pm5* and *mc2* appear to be absent (Ragsdale et al., 2011). As well, in the pharynx of a stylet-bearing species of Panagrolaimomorpha, *Aphelenchoides blastophthorus*, all marginal and radial cells posterior to its very short isthmus may be missing or greatly reduced in size (Ragsdale et al., 2011; Shepherd et al., 1980, 1984; Geraert, 1997). The posterior pharynx is important for its taxonomic characters and for understanding the evolution of the pharynx in the Rhabditida, and further work using fluorescent

staining of cell boundaries in this little investigated region should be fruitful.

### Adaptation of the Cell Classes for Different Feeding Strategies

Figure 2 illustrates how, as proposed by De Ley et al. (1995), a conserved ordered set of cell classes can be modified to produce different stoma architectures and functions. Cell diameter and length are varied, placing cuticular structures into different positions, and expression of muscle is varied, giving regions different functions. These are examples of relatively simple cuticular structures adapted for bacteria feeding. Strikingly different structures are produced for other types of feeding. The best documented of these include representatives of Tylenchomorpha and Aphelenchoididae (Panagrolaimomorpha), in which the stoma contains a cuticular stylet that is protruded through a sleeve in the cheilostom by protractor muscles, a specialization primarily for feeding on fungal or plant cells. A TEM-based 3D reconstruction of the anterior pharynx of *Aphelenchus avenae* (Tylenchomorpha) documented the homology of the cell classes with that of *C. elegans*, including the conserved sequence along the luminal cuticle (Ragsdale et al., 2011). However, the cuticular structures they form and muscular functions are very different. The stylet cone and shaft are formed during a molt by *a1* and *a2* and the three stylet knobs at the base of the stylet are formed by the unpaired *e1* cells. The anterior branch of each *e1* becomes one of the three protractor muscles while the posterior half, with *e3*, forms a non-muscular tube like that produced by *e1* and *e3* in *C. elegans* (Baldwin and Hirschmann, 1976; Endo, 1985; Ragsdale et al., 2008, 2011). As in *C. elegans*, marginal cell *e2* is associated successively with *e1*, *e3*, *pm1*, and *pm2* (Fig. 8), and marginal cell *mc1* is with *pm3-4* and *mc2* is with *pm5*. As in *C. elegans*, *pm1* cells appear to have a constraining function since the myofilaments are oriented circumferentially, except that these cells are not fused in *A. avenae*. The thin *pm2* “valve” muscles in *A. avenae*, as in *C. elegans*, insert in the region of the *dgo* where they would open the tricuspid valve. *Pm3* cells, which cover the entire length of the procorpus of *C. elegans*, are reduced to very thin “valve” muscles in *A. avenae* that insert posterior to the *dgo*. The function of *pm4* and *pm5* cells is homologous to those in *C. elegans* as pumping muscles in the bulb and isthmus, respectively.

The same cell class pattern of the stoma and procorpus occurs in the major basal clade Enoplida (Fig. 1). Muscular *e1* and *e3* cells function to operate three cuticular rod-like jaws in the stoma, pulling in obliquely anterior and posterior directions. In TEMs of the predator *Rhabdodema minima* published by Hope (1988), one can

recognize *e1*, *e3* and *pm1* associated with marginal cells *e2*. Contraction of the muscular *e1* cells would pull the lower buccal capsule obliquely forward, a motion that would widen the oral opening and move small teeth (odontia) to the opening (Hope, 1988).

### Future Applicability

Fluorescent-antibody staining of AJs in epithelial cell boundaries, examined by either epifluorescence or confocal microscopy, may have particular value in elucidating phenotypic evolution among nematode taxa. We have demonstrated the additional value of confocal microscopy for accurately reconstructing the stoma architecture in 3D. The resulting multifocal series of microscopic images of a species, made available as a through-focus movie, can be taxonomically informative (De Ley et al., 2005; Fig 7 legend). Several characters in the stoma are revealed: the homology of the sequential cell classes, the variation of diameter and extent of the cells along the lumen and a possible homology in what cells express certain cuticular structures such as the *dgo*, valves and sensory nerve terminals. Muscle function of stoma cells may be visualized by staining with fluorescein-conjugated phalloidin to locate presence and orientation of myofilaments (Shaham, 2006). Fluorescent labeling approaches would facilitate the exploration of cellular architecture in other taxa and need to be extended to the posterior pharynx in taxa already investigated. Fluorescent staining of epithelial cell boundaries should also be useful in comparisons among taxa of the processes involved in stoma formation during embryogenesis and molting. This would be a natural extension of work being done on the developing pharyngeal tube in *C. elegans* embryos (Mango, 2009; Rasmussen et al., 2013).

Also, fluorescent labeling of AJs have potential for comparisons of the cellular architecture of other epithelial tissues. Examples of MH27-labeled tissues include the posterior pharynx and valve (Rasmussen et al., 2008, 2012, 2013), hypodermis (Podbilewicz and White, 1994), male tail (Fitch and Emmons, 1995), vulva (Sharma-Kishore et al., 1999) and sensory organs (this study). Comparative studies of these organs in other taxa have usually been done by DIC microscopy. However, Fitch and co-workers combined DIC observations of ray structure with epifluorescence of MH27-labeled cell boundaries in their comparison of species closely related to *C. elegans*. They showed, for example, that the positions of hypodermal and ray cells in larvae determine the elaborate and diverse architecture of adult male tails (Fitch and Emmons, 1995; Fitch, 1997).

Since body form and organ structure are often based on epithelial cells, marking cell boundaries

by fluorescent-antibody staining of apical junctions should be useful in other transparent animals.

## AUTHOR CONTRIBUTIONS

Jay Burr designed and analyzed the experiments and wrote the article. Jim Baldwin conceived of the project, provided lab space and supplies and contributed to revisions.

## ACKNOWLEDGMENTS

The MH27 antibody was kindly donated by David Fitch and instruction in the use of the confocal microscope was provided by David Carter of the Microscopy Core Instrumentation Facility at UCR. The Perkins longitudinal TEM prints were donated by Edward Hedgecock to the Baldwin lab where they were scanned for posting on the WormImage Database, [www.WormImage.org](http://www.WormImage.org) (supported by NIH grant OD 010943 to David Hall). Higher resolution images from the *C. elegans* N2T series than those downloadable from WormImage Database website were kindly provided by David Hall. The authors thank Paul De Ley and Einhard Schierenberg for critically reading the manuscript and anonymous reviewers for valuable suggestions. Jay Burr's travel expenses came from a retirement research fund bequeathed by his mother, Phyllis Carter Burr.

## LITERATURE CITED

- Albertson DG, Thomson JN. 1976. The pharynx of *Caenorhabditis elegans*. *Philos Trans R Soc Lond B* 275:299–325. doi: 10.1098/rstb.1976.0085)
- Altun ZF, Hall DH. 2009. Alimentary System, Pharynx. In: *WormAtlas*. doi:10.3908/wormatlas.1.3 Edited for the web by Herndon LA. Last revision: July 21, 2012.
- Baldwin JG, Hirschmann H. 1976. Comparative fine structure of the stomatal region of males of *Meloidogyne incognita* and *Heterodera glycines*. *J Nematol* 8:1–17.
- Baldwin JG, Eddleman CD. 1995. Buccal capsule of *Zeldia punctata* (Nemata: Cephalobidae): An ultrastructural study. *Can J Zool* 73:648–656.
- Baldwin JG, Souza RM, Dolinski CM. 2001. Fine structure and phylogenetic significance of a muscular basal bulb in *Basiria gracilis* Thorne, 1969 (Nematoda: Tylenchidae). *Nematology* 3:681–688.
- Baldwin JG, Ragsdale EJ, Bumbarger D. 2004. Revised hypotheses for phylogenetic homology of the stomatostylet in tylenchid nematodes. *Nematology* 6:623–632.
- Bert W, Leliaert F, Vierstraete AR, Vanfleteren JR, Borgonie G. 2008. Molecular phylogeny of the Tylenchina and evolution of the female gonoduct (Nematoda: Rhabditida). *Mol Phylogenet E* vol 48:728–744.
- Bik HM, Lambshead PJD, Thomas WK, Lunt DH. 2010. Moving towards a complete molecular framework of the Nematoda: A focus on the Enoplida and early-branching clades. *BMC Evol Biol* 10:353.
- Blaxter M, De Ley P, Garey JR, Liu LX, Scheldeman P, Vierstraete A, Vanfleteren JR, Mackey LY, Dorris M, Frisse LM, Vida JT, Thomas WK. 1998. A molecular evolutionary framework for the phylum Nematoda. *Nature* 392:71–75.
- Bossinger O, Klebes A, Segbert C, Theres C, Knust E. 2001. Zonula adherens formation in *Caenorhabditis elegans* requires dlg-1, the homologue of the *Drosophila* gene discs large. *Devel Biol* 230:29–42.
- Brenner S. 1974. The genetics of *Caenorhabditis elegans*. *Genetics* 77:71–94.
- Bumbarger DJ, Crum J, Ellisman MH, Baldwin JG. 2006. Three-dimensional reconstruction of the nose epidermal cells in the microbial feeding nematode. *Acrobeles complexus* (Nematoda: Rhabditida). *J Morphol* 267:1257–1272.
- Bumbarger DJ, Crum J, Ellisman MH, Baldwin JG. 2007. Three-dimensional fine structural reconstruction of the nose sensory structures of *Acrobeles complexus* compared to *Caenorhabditis elegans* (Nematoda: Rhabditida). *J Morphol* 268: 649–663.
- Centonze V, Pawley JB. 2006. Tutorial on practical confocal microscopy and use of the confocal test specimen. In: Pawley JB, SpringerLink (Online service), editors. *Handbook of Biological Confocal Microscopy*, 3rd ed. New York: Springer.
- Chalfie M, Tu Y, Euskirchen, Ward WW Prasher DC. 1994. Green fluorescent protein as a marker for gene expression. *Science*, New Series 263:802–805.
- Chitwood, BG, Chitwood, MBH. 1950. *Introduction to Nematology*. Baltimore: University Park Press. 334 p.
- Cole TS, Schierenberg E. 1986. Laser microbeam-induced fixation for electron-microscopy - visualization of transient developmental features in nematode embryos. *Experientia* 42: 1046–1048.
- Collins TJ. 2007. ImageJ for microscopy. *BioTechniques* 43:S25–S30.
- Coomans A. 2000. Nematode systematics: Past, present and future. *Nematology* 2:3–7.
- De Ley P. 2006. A quick tour of nematode diversity and the backbone of nematode phylogeny (January 25, 2006). In: *WormBook*. The *C. elegans* Research Community, editors. pp 1–8. doi/10.1895/wormbook.1.41.1, <http://www.wormbook.org>.
- De Ley P, Blaxter M. 2002. Systematic position and phylogeny. In: Lee DL, editor. *The Biology of Nematodes*. London: Taylor & Francis. pp 1–30.
- De Ley P, Van de Velde MC, Mounport D Baujard P, Coomans 1995. Ultrastructure of the stoma in Cephalobidae, Panagrolaimidae, and Rhabditidae, with a proposal for a revised stoma terminology in Rhabditida (Nematoda). *Nematologica* 41:153–182.
- De Ley P, De Ley IT, Morris K, Abebe E, Mundo-Ocampo M, Yoder M, Heras J, Waumann D, Rocha-Olivares A, Burr AHJ, Baldwin JG, Thomas WK. 2005. An integrated approach to fast and informative morphological vouchering of nematodes for applications in molecular barcoding. *Philos Trans R Soc B-Biol Sci* 360:1945–1958.
- Dolinski CM, Baldwin JG. 2003. Fine structure of the stoma of *Bunonema* sp. and *Teratorhabditis palmarum* (Nematoda) and its phylogenetic significance. *J Nematol* 35:244–251.
- Dolinski C, Borgonie G, Schnabel R, Baldwin JG. 1998. Buccal capsule development as a consideration for phylogenetic analysis of Rhabditida (Nemata). *Dev Genes E* vol 208:495–503. doi:10.1007/s004270050208)
- Endo BY. 1985. Ultrastructure of the head region of molting second-stage juveniles of *Heterodera glycines* with emphasis on stylet formation. *J Nematol* 17:112–123.
- Feng D, Marshburn D, Jen D, Weinberg RJ, Taylor RM II, Burette A. 2007. Stepping into the third dimension. *J Neuroscience* 27:12757–12760.
- Finney M, Ruvkun G. 1990. The *unc-86* gene-product couples cell lineage and cell identity in *C. elegans*. *Cell* 63:895–905.
- Fitch DHA. 1997. Evolution of male tail development in rhabditid nematodes related to *Caenorhabditis elegans*. *Syst Biol* 46:145–179.
- Fitch DHA, Emmons SW. 1995. Variable cell positions and cell contacts underlie morphological evolution of the rays in the male tails of nematodes related to *Caenorhabditis elegans*. *Dev Biol* 170:564–582. doi:10.1006/dbio.1995.1237)
- Francis F, Waterston RH. 1991. Muscle cell attachment in *Caenorhabditis elegans*. *J Cell Biol* 114:465–479.

- Geraert E. 1997. Comparison of the oesophageal structure in *Aphelenchoides* and *Hoplolaimus* (Tylenchida: Nematoda). *Nematologica* 43:295–305.
- Grootaert P, Coomans A. 1980. The formation of the anterior feeding apparatus in dorylaims. *Nematologica* 26:406–431.
- Hedgecock EM, Culotti JG, Hall DH. 1990. The *unc-5*, *unc-6*, and *unc-40* genes guide circumferential migrations of pioneer axons and mesodermal cells on the epidermis in *C. elegans*. *Neuron* 2:61–85.
- Hirumi H, Chen TA, Lee KJ, Maramorosh K. 1968. Ultrastructure of the feeding apparatus of the nematode *Trichodorus christiei*. *J Ultrastruct Res* 24:434–453.
- Holterman M, Van Der Wurff A, Van Den Elsen S, Van Megen H, Bongers T, Holovachov O, Bakker J, Helder J. 2006. Phylum-wide analysis of SSU rDNA reveals deep phylogenetic relationships among nematodes and accelerated evolution toward crown clades. *Mol Biol Evol* 23:1792–1800.
- Hope DW. 1988. Ultrastructure of the feeding apparatus of *Rhabdodemania minima* Chitwood, 1936 (Enoplida: Rhabdodemaniidae). *J Nematol* 20:118–140.
- Hutter H. 2012. Fluorescent protein methods: Strategies and applications. *Method Cell Biol* 107:67–92.
- Kiontke K, Fitch DHA. 2005. The phylogenetic relationships of *Caenorhabditis* and other rhabditids. In: The *C. elegans* Research Community, editor. *WormBook*. pp 1–11. doi/10.1895/wormbook.1.11.1, <http://www.wormbook.org>. [PubMed].
- Kiontke K, Fitch DHA. 2013. Nematodes. *Curr Biol* 23:R862–R864.
- Kolotuev I, Podbilewicz B. 2004. *Pristionchus pacificus* vulva formation: Polarized division, cell migration, cell fusion and evolution of invagination. *Dev Biol* 266:322–333.
- Kolotuev I, Podbilewicz B. 2008. Changing of the cell division axes drives vulva evolution in nematodes. *Dev Biol* 313:142–154.
- Köppen M, Simske JS, Sims PA, Firestein BL, Hall DH, Radice AD, Rongo C, Hardin JD. 2001. Cooperative regulation of AJM-1 controls junctional integrity in *Caenorhabditis elegans* epithelia. *Nat Cell Biol* 3:983–991.
- Labouesse M. 2006. Epithelial junctions and attachments (January 13, 2006). In: The *C. elegans* Research Community, editors. *WormBook*. pp 1–21. (doi/10.1895/wormbook.1.56.1, <http://www.wormbook.org>)
- Maggenti AR. 1981. Nematodes: Development as plant parasites. *Annu Rev Microbiol* 35:135–154.
- Mango SE. 2007. The *C. elegans* pharynx: A model for organogenesis. In: The *C. elegans* Research Community, editors. *WormBook*. pp 1–26. (doi/10.1895/wormbook.1.129.1, <http://www.wormbook.org>)
- Mango SE. 2009. The molecular basis of organ formation: Insights from the *C. elegans* foregut. *Annu Rev Cell Dev Biol* 25:597–628.
- Meldal BHM, Debenham NJ, De Ley P, De Ley IT, Vanfleteren JR, Vierstraete AR, Bert W, Borgonie G, Moens T, Tyler PA, Austen MC, Blaxter ML, Rogers AD, Lamshead PJ. 2007. An improved molecular phylogeny of the Nematoda with special emphasis on marine taxa. *Mol Phylogenet Evol* 42:622–636.
- Mello CC, Kramer JM, Stinchcomb D, Ambros V. 1991. Efficient gene transfer in *C. elegans*: Extrachromosomal maintenance and integration of transforming sequences. *Embo J* 10:3959–3970.
- Michaux G, Legouis R, Labouesse M. 2001. Epithelial biology: Lessons from *Caenorhabditis elegans*. *Gene* 277:83–100.
- Perkins LA, Hedgecock EM, Thomson JN, Culotti JG. 1986. Mutant sensory cilia in the nematode *Caenorhabditis elegans*. *Dev Biol* 117:456–487.
- Podbilewicz B. 2006. Cell fusion. In: The *C. elegans* Research Community, editors. *WormBook*, doi/10.1895/wormbook.1.52.1, <http://www.wormbook.org>.
- Podbilewicz B, White JG. 1994. Cell fusions in the developing epithelia of *C. elegans*. *Dev Biol* 161:408–424.
- Portereiko MF, Mango SE. 2001. Early morphogenesis of the *Caenorhabditis elegans* pharynx. *Dev Biol* 233:482–494.
- Portereiko MF, Saam J, Mango SE. 2004. ZEN-4/MKLP1 is required to polarize the foregut epithelium. *Curr Biol* 14:932–941.
- Ragsdale EJ, Baldwin JG. 2010. Resolving phylogenetic incongruence to articulate homology and phenotypic evolution: A case study from Nematoda. *Proc R Soc B* 277:1299–1307.
- Ragsdale EJ, Crum J, Ellisman MH, Baldwin JG. 2008. Three-dimensional reconstruction of the stomatostylet and anterior epidermis in the nematode *Aphelenchus avenae* (Nematoda: Aphelenchidae) with implications for the evolution of plant parasitism. *J Morphol* 269:1181–1196.
- Ragsdale EJ, Ngo PT, Crum J, Ellisman MH, Baldwin JG. 2011. Reconstruction of the pharyngeal corpus of *Aphelenchus avenae* (Nematoda: Tylenchomorpha), with implications for phylogenetic congruence. *Zool J Linn Soc* 161:1–30.
- Ragsdale EJ, Kanzaki N, Röseler W, Herrmann M, Sommer RJ. 2013. Three new species of *Pristionchus* (Nematoda: Diplogastriidae) show morphological divergence through evolutionary intermediates of a novel feeding-structure polymorphism. *Zool J Linn Soc Lond* 168:671–698.
- Raski DJ, Jones NO, Roggen DR. 1969. On the morphology and ultrastructure of the esophageal region of *Trichodorus allius* Jensen. *Proc Helminthol Soc Wash* 36:106–118.
- Rasmussen JP, English K, Tenlen JR, Priess JR. 2008. Notch signaling and morphogenesis of single-cell tubes in the *C. elegans* digestive tract. *Dev Cell* 14:559–569.
- Rasmussen JP, Reddy SS, Priess JR. 2012. Laminin is required to orient epithelial polarity in the *C. elegans* pharynx. *Development* 139:2050–2060.
- Rasmussen JP, Feldman JL, Reddy SS, Priess JR. 2013. Cell interactions and patterned intercalations shape and link epithelial tubes in *C. elegans*. *PLoS Genet* 9:1–22.
- Shaham S. 2006. Editor: *WormBook: Method Cell Biology* (January 02, 2006). *WormBook*, ed. The *C. elegans* Research Community. doi/10.1895/wormbook.1.49.1, <http://www.wormbook.org>.
- Shakes DC, Miller DM, Nonet ML. 2012. Immunofluorescence Microscopy. In: Rothman JL, Samuel Singson S, editors. *Method Cell Biology*, Vol. 107. New York: Academic Press. pp 35–66.
- Sharma-Kishore R, White JG, Southgate E, Podbilewicz B. 1999. Formation of the vulva in *Caenorhabditis elegans*: A paradigm for organogenesis. *Development* 126:691–699.
- Shemer G, Suissa M, Kolotuev I, Nguyen KCQ, Hall DH. 2004. EFF-1 is sufficient to initiate and execute tissue-specific cell fusion in *C. elegans*. *Curr Biol* 14:1587–1591.
- Shepherd AM, Clark SA, Hooper DJ. 1980. Structure of the anterior alimentary tract of *Aphelenchoides blastophthorus* (Nematoda: Tylenchida, Aphelenchina). *Nematologica* 26:313–357.
- Shepherd AM, Perkins WL, Green RJ, Clark SA. 1984. A study of oesophageal structure in a nematode, *Aphelenchoides blastophthorus* (Aphelenchida), using computer graphics reconstruction from serial thin sections. *J Zool Lond* 204:271–288.
- Sibarita J-B. 2005. Deconvolution microscopy. *Adv Biochem Engin/Biotechnol* 95:201–243.
- Siddiqi MR. 2000. Tylenchida: Parasites of Plants and Insects, 2nd ed. Wallingford: CABI Publishing. 833 p.
- Simske JS, Hardin J. 2001. Getting into shape: Epidermal morphogenesis in *Caenorhabditis elegans* embryos. *Bioessays* 23:12–23.
- Smythe AB. 2015. Evolution of feeding structures in the marine nematode order Enoplida. *Integr Compar Biol* 55:228–240.
- Sudhaus W, Kiontke K. 1996. Phylogeny of *Rhabditis* subgenus *Caenorhabditis* (Rhabditidae, Nematoda). *J Zool Syst Evol Res* 34:217–233.
- Sulston JE, Horvitz HR. 1977. Post-embryonic cell lineages of the nematode, *Caenorhabditis elegans*. *Dev Biol* 56:110–156.
- Sulston JE, Schierenberg E, White JG, Thomson JN. 1983. The embryonic cell lineage of the nematode *Caenorhabditis elegans*. *Dev Biol* 100:64–119.
- van Megen H, van den Elsen S, Holterman M, Karssen G, Mooyman P, Bongers T, Holovachov O, Bakker J, Helder J. 2009. A phylogenetic tree of nematodes based on about 1200 full-length small subunit ribosomal DNA sequences. *Nematology* 11:927–950.

- White J G, Amos W B, Fordham M. 1987. An evaluation of confocal versus conventional imaging of biological structures by fluorescence light microscopy. *J Cell Biol* 105:41–48.
- Wright KA, Thomson JN. 1981. The buccal capsule of *Caenorhabditis elegans* (Nematoda: Rhabditoidea): An ultrastructural study. *Can J Zool* 59:1952–1961.
- Zhang YC, Baldwin JG. 1999. Ultrastructure of the esophagus of *Diplenteron* sp. (Diplogasterida) to test hypotheses of homology with Rhabditida and Tylenchida. *J Nematol* 31:1–19.
- Zhang YC, Baldwin JG. 2000. Phylogenetic implications of ultrastructure of the post-corpus of *Zeldia punctata* (Cephalobina) with comparisons to *Caenorhabditis elegans* (Rhabditina) and *Diplenteron* sp. (Diplogastrina). *Philos Trans R Soc Lond B* 267:1229–1238.
- Zhang YC, Baldwin JG. 2001. Ultrastructure of the postcorpus of the esophagus of *Teratocephalus lirellus* (Teratocephalida) for interpreting character evolution in Secernentea (Nematoda). *Can J Zool* 79:16–25.